Adaptive Responses to PARP Inhibition Predict Response to Olaparib and Durvalumab: Multi-omic Analysis of Serial Biopsies in the AMTEC Trial

Zahi I. Mitri[1,2,†], Allison L. Creason[3,4,†], Jayne M. Stommel[3,†], Daniel Bottomly[3], Tugba Y. Ozmen[3,6], Matthew J. Rames[3,6], Furkan Ozmen[3,6], Boyoung Jeong[3,6], Natalia Lukashchuk[7], Jack Ashton[7], Jeong Youn Lim[5], Shamilene Sivagnanam[6], Konjit Betra[6], Jinho Lee[3,8], Marilyne Labrie[9-11], SMMART Clinical Trials Program[3], Lisa M. Coussens[3,6], Christopher L. Corless[3,8], Shannon K. McWeeney[3,12], Gordon B. Mills[3,6*]

[1]British Columbia Cancer Agency, Vancouver, BC, Canada

[2]Division of Medical Oncology, University of British Columbia, Vancouver, BC, Canada

[3]Knight Cancer Institute, Oregon Health & Science University, Portland, OR, USA

[4]Department of Biomedical Engineering, Oregon Health & Science University, Portland, OR, USA

[5]Biostatistics Shared Resource, Oregon Health & Science University, Portland, OR, USA

[6]Department of Cell, Developmental and Cancer Biology, Oregon Health & Science University, Portland, OR, USA

[7]Translational Medicine, Oncology Research and Development (R&D), AstraZeneca, Cambridge, United Kingdom

[8]Knight Diagnostic Laboratories, Oregon Health & Science University, Portland, OR, USA

[9]Department of Immunology and Cell Biology, Faculty of Medicine and Health Sciences, Université de Sherbrooke, Sherbrooke, Canada

[10]Centre de Recherche du Centre Hospitalier de l'Université de Sherbrooke (CRCHUS), Sherbrooke, Canada

[11]Institut de Recherche sur le Cancer de l'Université de Sherbrooke (IRCUS), Sherbrooke, Canada

[12]Division of Bioinformatics and Computational Biology, Department of Medical Informatics and Clinical Epidemiology, Oregon Health & Science University, Portland, OR, USA

[†]These authors contributed equally to this work.

*Corresponding Author

Abstract

In syngeneic murine breast cancer models, poly ADP-ribose polymerase inhibitor (PARPi) and anti-PD-L1 combinations induce deep, sustained responses independent of *BRCA1/2* mutation status. We therefore investigated this combination in the AMTEC clinical trial, in which a one-month olaparib run-in was followed by combined olaparib and durvalumab in participants with *BRCA1/2* wild-type metastatic triple negative breast cancer. To characterize adaptive responses to olaparib monotherapy, paired biopsies taken before and during PARPi lead-in were deeply characterized by DNA, RNA, and protein multi-omic analyses, including spatially-resolved single cell proteomics for tumor and immune contexture. We identified multiple potential tumor-intrinsic and microenvironmental biomarkers from pre-treatment and on-olaparib biopsies that robustly predicted participant response to combined olaparib and durvalumab. Notably, the on-olaparib biopsy provided the greatest information content, suggesting that adaptation of malignant cells and the tumor ecosystem to PARPi can serve as a predictor of potential benefit from combined PARPi and anti-PD-L1 therapy.

Introduction

Triple negative breast cancer (TNBC), comprising 15-20% of all breast cancers, predominantly affects younger women and certain ethnic groups. Compared to other breast cancer subtypes, TNBC is characterized by aggressive features, a higher propensity for metastasis, and an overall worse prognosis[1]. Despite advancements in understanding TNBC biology, outcomes for metastatic TNBC (mTNBC) remain poor, with an overall survival of 1-2 years with standard therapies[2-4].

The DNA damage response (DDR) pathway is frequently dysregulated in TNBC, with nearly half of all cases exhibiting aberrations. *BRCA1/2* mutations are observed in about 15% of TNBC, while another 45% of TNBC with genomic instability have wild type *BRCA1/2*, suggesting that other aberrations can lead to defects in this pathway[1,5-7]. DDR dysregulation renders TNBC sensitive to DNA damaging therapies such as chemotherapy, radiation therapy, and more recently, PARP inhibitors (PARPi). PARPi are of particular interest in mTNBC because of the high frequency of defects in homologous recombination repair, the high-fidelity repair pathway for double-stranded DNA breaks[8].

In mTNBC, the PARP inhibitors olaparib and talazoparib, FDA-approved for patients with germline *BRCA1/2* mutations, improve clinical outcomes primarily by exploiting synthetic lethality with HRD. However, even in this population, responses to PARPi monotherapy are often short-lived, with most patients eventually experiencing disease progression[9,10]. Moreover, PARPi monotherapy has limited activity in *BRCA1/2* wild-type *(BRCA1/2^{wt})* tumors, which constitute the majority of mTNBC[11], with the VIOLETTE trial showing minimal benefit in these patients[12]. Preclinical and early clinical data suggest that PARPi combination therapies are safe and more effective in *BRCA1/2^{wt}* TNBC, highlighting potential opportunities for these treatments for this population[13-15].

Immune checkpoint blockade (ICB) has improved outcomes for various tumor types, especially those with high tumor mutational burden (TMB) and neoantigenic propensity, which can bolster anti-tumor immunity[16,17]. In mTNBC, the combination of the programmed death-1 (PD-1) inhibitor pembrolizumab and chemotherapy is FDA-approved for patients with tumors expressing programmed death ligand 1 (PD-L1). However, this indication excludes the majority of mTNBCs, which are frequently PD-L1 negative, and clinical benefit is frequently brief even in PD-L1 positive patients[18]. Additionally, TMB in TNBC is usually below the generally accepted 10 mutations/Mb that predicts ICB efficacy in other cancer types[19].

Extensive preclinical data demonstrate that PARP inhibitors induce adaptive responses in malignant cells and the tumor ecosystem, including immune cells, in models of HRR-deficient and competent tumors[20-24]. Similar adaptive changes have been observed in human tumors, such as breast cancer, under therapeutic stress induced by PARPi[14,15,25,26]. While specific adaptive responses vary across patients, the number of stress responses engaged following PARPi appears to be limited, facilitating the identification of patient-specific adaptive responses. Targeting these adaptive responses – for example, by increasing PARPi-induced stress, blocking protective responses, or capitalizing on the rewiring of malignant cells and the immune microenvironment[27] – has the potential to improve responses to PARP therapies, including in *BRCA1/2*^{wt} TNBC. The identification of the specific adaptive response to target may require collecting tumor biopsies taken before and during PARPi monotherapy, then cataloguing drug-induced changes to exploit in a combined treatment regimen.

Combining PARPi with ICB is a promising therapeutic approach to leverage PARPi-induced adaptive changes in immune signaling. PARP inhibition enhances antigen presentation, recruits cytotoxic T lymphocytes, and activates the stimulator of interferon genes (STING) pathway[21,22,28], all of which could increase the efficacy of ICB. Notably, PARPi can activate the STING pathway in *BRCA1/2*^{wt} syngeneic cancer models that are DNA repair competent[23], potentially leading to an infiltration of adaptive immune cells that would recognize neoantigens generated through low fidelity DNA repair. Indeed, clinical trials combining ICB and PARPi showed activity in both *BRCA1/2*^{mut} and *BRCA1/2*^{wt} mTNBC, although response rates are lower in the wild-type group[14,29-31].

Building on these findings, we initiated the Adaptive Molecular Therapy of Evolving Cancers (AMTEC) trial to evaluate the efficacy of combining the PARP inhibitor olaparib with the PD-L1 inhibitor durvalumab in *BRCA1/2*^{wt} mTNBC[32]. This trial includes an olaparib monotherapy phase followed by a combination phase with olaparib and durvalumab, with biopsies collected at baseline and during olaparib monotherapy. Both biopsies are analyzed with a suite of multi-omic assays in an in-depth examination of changes in malignant cells and the tumor ecosystem in response to PARPi-mediated therapeutic stress. Using this approach, the AMTEC trial aims to identify adaptive changes induced by PARPi monotherapy that could serve as biomarkers for selecting patients likely to benefit from PARPi/ICB combination therapy. An additional aim is to discover resistance mechanisms to combined PARPi/ICB, which could be targeted with alternative PARPi combinations. Here we report the clinical and translational results of stage 1 of the AMTEC trial.

Results

AMTEC is a single-arm, open-label phase II trial assessing the efficacy of olaparib combined with durvalumab in participants with *BRCA1/2* wild type mTNBC (Fig. 1a). Eligible participants undergo a pre-treatment biopsy upon enrollment, followed by a 4-week olaparib treatment. At the end of this olaparib lead-in, all participants undergo a second biopsy on olaparib, and then durvalumab is added to the treatment regimen.

The primary endpoint of the study is the overall response rate (ORR) for olaparib plus durvalumab. Secondary endpoints include clinical benefit rate (CBR), duration of response, progression-free survival (PFS), and overall survival (OS), as well as safety and tolerability of the treatment.

Participant and Disease Characteristics

Seventeen participants with biopsy-proven mTNBC were enrolled in stage 1 of the AMTEC trial between January 2019 and May 2020. Participant characteristics are summarized in Table 1. All participants had an ECOG performance status of 0 or 1. Approximately equal numbers of participants had 0, 1, or 2 lines of prior therapy in the metastatic setting, including seven participants who had received platinum-based therapy. Four participants had brain metastases that were controlled at the time of enrollment.

Of the seventeen enrolled participants, two were replaced due to required discontinuation of study drugs, resulting in a set of fifteen participants in the primary endpoint ORR analysis (Extended Data Fig. 1a). An additional participant voluntarily withdrew during olaparib/durvalumab cycle 3 per personal preference. This participant ("M"; Fig. 1b) achieved a RECIST best response of partial response (PR) [33] on first restaging and was included in the ORR analysis but omitted from survival analyses, resulting in a total of fourteen participants evaluable for the survival efficacy endpoints (PFS and OS).

Efficacy Endpoints

Among the fifteen participants who received the combination therapy and were evaluable for the primary ORR efficacy endpoint, there were four PRs and no complete responses (CR), for an ORR of 27% (Fig. 1b and Extended Data Table 1a). An additional four participants had stable disease (SD) ≥6 months, for a CBR of 53%. A fifth participant ("G") had SD for 5.7 months.

The best percentage change from baseline for the sum of all target lesions was calculated for each evaluable participant (Fig. 1c). Among the five participants with SD as the best response, percentage changes ranged from 0% to -27%. For the four participants with PR as the best response, the range was from -30% to -40%. In contrast, the five participants with progressive disease (PD) showed percentage changes ranging from +23% to +165%. Participant N did not have target lesion size measurements taken at disease progression and percent change was therefore unevaluable.

The median PFS for the entire cohort was 5.52 months (95% CI 2.4 – 8.97 months), and median OS was 12.88 months (95% CI 4.17 – 17.77 months; Fig. 1d and Extended Data Table 1a). Participants with a best response of SD or PR did not show statistically significant differences in PFS or OS (data not shown). Therefore, for all further analyses, we combined SD and PR cases as participants who derived clinical benefit from the study therapy.

Participants with PR or SD had significantly better survival outcomes than those with PD (OS $p = 0.0013$, PFS $p < 0.0001$; Fig. 1e). The median survival times for participants with PR/SD were 9 months PFS (95% CI 5.72 – 10.12 months) and 17 months OS (95% CI 10.22 – 19.38 months), compared to 2 months PFS (95% CI 1.71 – 2.46 months) and 3 months OS (95% CI 1.94 – 7.98 months) for participants with PD as the best response.

Clinical outcomes were not associated with either the total number of therapies or prior platinum treatment in the metastatic setting (data not shown). Additionally, for participants with a history of CNS metastases, CNS progression occurred concurrently with the progression of extra-cranial systemic disease.

Safety Results

All seventeen participants who received at least one dose of study drugs were evaluable for safety endpoints (Extended Data Table 1b). Most treatment-related adverse events (AEs) were mild to moderate (grade 1-2 = 140/152; 91%). Ten participants (59%) experienced severe AEs (grade 3), with 14/33 (42%)

considered as possibly related to the study treatment. No grade 4 or 5 AEs attributed to study interventions or treatment were noted.

Among the grade 3 AEs, two occurred in participants with immune-related elevated liver enzymes attributed to durvalumab, which resolved following dose hold and supportive medications (Extended Data Table 1c). The most common olaparib-related grade 3 AE was anemia in 4/17 participants (24%), which resolved with a dose hold and adjustment per protocol. The two grade 5 AEs included a motor vehicle accident unrelated to treatment and a case of pain related to rapidly progressive disease.

Clinical and Exploratory Research Analytics

We conducted a comprehensive exploratory analysis of the tumor-intrinsic and microenvironmental biology of both the pre-treatment and on-olaparib tumor biopsies. This included a focus on signatures that emerged as adaptive responses to the olaparib monotherapy lead-in.

The methods used included: 1) clinical immunohistochemistry (IHC); 2) *GeneTrails*® DNA sequencing of 225 cancer-relevant genes; 3) whole exome DNA sequencing (WES); 4) bulk transcriptomic sequencing (RNAseq) for gene rearrangements and RNA expression levels; 5) NanoString GeoMx® Digital Spatial Profiling (DSP) of 48 proteins and phospho-proteins; 6) reverse phase protein arrays (RPPA) of 480 proteins and post-translational modifications; 7) RAD51 foci analysis to detect homologous recombination deficiency, and 8) multiplexed immunohistochemistry (mIHC) with 23 antibodies to quantify infiltrating immune cells and their functional states. Due to sample availability and assay-specific tumor content requirements, not all assays were performed on every sample, and some mIHC assays failed due to tissue loss during analysis.

Extended Data Fig. 1b and Extended Data Table 1d summarize the results from these clinical and exploratory research analytics, discussed in detail below. Extended Data Fig. 1b shows clinical metadata for each sample, along with data resulting from each of the assays listed above, noting statistical significance and associations with best response (R), PFS (P), OS (O), and/or changes between paired biopsies (B). Extended Data Table 1d lists the statistically significant features that predict response to the olaparib/durvalumab combination, using Boruta and Bonferroni multiple comparison adjustment within each data type.

Tumor-Intrinsic Analytes

The following tumor-intrinsic measurements did not show statistically significant correlations with participant outcomes:1) mutations in *TP53*, the HRD pathway, or the MAPK pathway; 2) TMB (no sample exceeded 10 mutations/Mb); 3) percentage of malignant cells expressing PD-L1 or Ki-67 by IHC; 4) AR positivity by IHC or DSP; 5) biopsy site; or 6) tumor content, although this tended to be higher in participants with PD.

PD-L1 tumor cell positivity was assessed by IHC using two different cutoffs due to discrepancies in the literature[34]. PD-L1 tumor proportion scores ≥10% were observed in at least one biopsy from four of the fifteen participants, including three of nine (33%) demonstrating clinical benefit (PR/SD) and one of six (17%) participants who did not (PD; Extended Data Fig. 1b). PD-L1 scores ≥1% were observed in at least one biopsy from ten of the fifteen participants, including seven of nine (78%) demonstrating benefit (PR/SD) and three of six (50%) who did not (PD). Although not statistically significant, participants with

PD-L1 ≥1% were more likely to achieve PR/SD, aligning with other studies indicating an association between PD-L1 positivity and response to ICB in TNBC[35,36].

PD-L1 protein levels were also measured by NanoString DSP. Unlike IHC, high DSP protein levels in the pre-treatment biopsy, but not the on-olaparib biopsy, showed a statistically significant association with OS (pre-treatment p=0.03; see Extended Data Fig. 4o). The differences in statistical significance between IHC and DSP may be attributed to the greater quantitative sensitivity of DSP, variations in cutoff values for positive sample calls, or slight differences in sample sets. Thus, while PD-L1 may have influenced the response to olaparib and durvalumab, PD-L1 protein measurements by IHC are insufficient to accurately predict response.

Interestingly, olaparib-induced increases in the number of PD-1^+ cells, but not in PD-$L1^+$ cells, were significantly associated with achieving clinical benefit (PR/SD) from combined olaparib/durvalumab, as measured by mIHC (see Fig. 6a; Extended Data Fig. 6b). High PD-1^+ cells in the on-olaparib biopsy also showed a trend toward significance for OS (p=0.1, data not shown).

The most frequently mutated gene was *TP53*, observed in 14 out of 15 participants (93%). No tumor had a deleterious aberration in *BRCA1*, *BRCA2, BARD1, PALB2, RAD51C, or RAD51D*, which are known to confer sensitivity to PARPi[37,38] (Extended Data Fig. 1b). However, there were alterations in two other genes involved in homologous recombination (HR): a potentially pathogenic germline *ATM* mutation in Participant A and a potentially clinically significant somatic *CDK12* mutation in Participant G. Regarding mutations possibly related to durvalumab response, Participants E and F had deleterious mutations in *beta-2-microglobulin (B2M)*, and Participant K had a low frequency *JAK1* mutation detected only in the on-olaparib biopsy.

PI3K/AKT pathway alterations were present in biopsies from two of nine PR/SD participants and in five of six PD participants. Note that Participant N had only one of the two biopsies with clinically reported *PTEN* loss, possibly due to tumor content variability constraining copy number loss detection. Receptor tyrosine kinase or MAPK pathway aberrations were present in only two participants: one with SD and one with PD as best response.

RPPA proteomics data were generated from a subset of samples: 9 pre-treatment biopsies, 8 on-treatment biopsies, and 7 matched pairs. Protein PARylation (PAR), which is catalyzed by PARP upon binding single-strand DNA breaks, was elevated in all evaluable pre-treatment biopsies from PD participants, but in only one PR/SD sample (Participant F) (Fig. 2a; Extended Data Fig. 1c). Although PAR was initially high in the PD samples, it significantly decreased to levels similar to those in the PR/SD samples upon olaparib treatment (Fig. 2a). This indicates that the poor response to the olaparib/durvalumab combination in these participants was not due to insufficient olaparib activity. No other proteins or protein pathways assessed by RPPA were associated with treatment outcomes, likely due to the limited number of samples with sufficient material for analysis.

Defects in HR are well-established predictive biomarkers for PARPi response, even in the absence of BRCA1/2 mutations[39-42]. To assess HR deficiency in our *BRCA1/2^{wt}* samples, we developed an immunofluorescence-based assay that distinguishes HR-competent (HRC) and HR-deficient (HRD) cells. Cells in G2 phase were evaluated for the presence of functional HR repair complexes and double-strand DNA breaks within the same nuclei, then samples were categorized as predominantly HRC, HRD, or

Intermediate (Extended Data Fig. 1b-e). Although HRC or HRD status alone was insufficient to predict clinical outcomes, the two participants with tumors classified as HRD (Participants M and E) achieved a best response of either PR or SD. In contrast, no analyzable samples from participants with PD were classified as HRD.

Genomic scarring is a common indicator of HRD due to its strong association with *BRCA1/2* mutations and other DNA damage mechanisms[43]. Given its association with HRD, we assessed the predictive value of the MutSig3 signature in the WES from the pre-therapy biopsy. Interestingly, MutSig3 was significantly associated with OS (p-val = 0.03; Fig. 2b) but not with best response or PFS (data not shown).

PI3K-AKT and RTK-MAPK pathway activity is associated with therapeutic resistance, including to PARPi and ICB[15,44,45]. To evaluate whether activation of these pathways influenced the response to olaparib/durvalumab in AMTEC, we catalogued PI3K-AKT and RTK-MAPK gene alterations and pathway activation via NanoString DSP phosphoprotein profiling.

Samples with elevated phosphoproteins in the PI3K-AKT pathway (indicative of PI3K-AKT pathway activation) tended to also have PI3K-AKT gene aberrations: six of the seven pathway-activated samples had a concurrent pathway gene alteration (Extended Data Fig. 1b). Consistent with the notion that PI3K-AKT gene alterations may be leading to pathway activation, in either biopsy, gene alterations or pathway activation were associated with poor outcomes: gene alterations with progressive disease and reduced OS and PFS, and pathway activation with reduced PFS (Extended Data Fig. 2a-c). Additionally, a combined analysis of samples with a mutation and/or elevated pathway activity showed an association with progressive disease and reduced OS and PFS (Fig. 2c; Extended Data Fig. 2d).

In contrast, RTK-MAPK DSP pathway activation was independent of gene alteration: none of the four pathway-activated samples had concurrent pathway mutations, and none of the three samples with genomic alterations also had pathway activation (Extended Data Fig. 1b). Consistent with our previous studies[15,26], MAPK pathway activation appeared to be induced by PARPi, as all four pathway-activated samples were from on-olaparib biopsies. MAPK pathway activation in the on-olaparib biopsy but not the pre-treatment biopsy was associated with worse OS and PFS (on-olaparib p-value = 0.03 for OS and 0.004 for PFS; Fig. 2d; Extended Data Fig. 2e).

Elevated signaling activity in the on-olaparib biopsy in either the PI3K-AKT or RTK-MAPK pathway strongly indicated poor clinical outcomes, including OS, PFS, and RECIST best response (on-olaparib p-values of 0.005, 0.003, and 0.015, respectively; Fig. 2e; Extended Data Fig. 2f). One or both pathways were activated in four of six PD participants but not in any PR/SD participants (Extended Data Fig. 1b). In contrast, gene alterations in either pathway in the on-olaparib biopsy did not significantly associate with response (on-olaparib p-value = 0.1 for OS, 0.12 for PFS, and 0.103 for best response; Extended Data Fig. 2g and data not shown). This suggests that protein-based analyses from on-treatment biopsies may be more informative for anticipating resistance to olaparib/durvalumab driven by PI3K-AKT or RTK-MAPK signaling in mTNBC.

Tumor Microenvironment Analyses

We also evaluated the tumor microenvironment in pre-treatment and olaparib-treated samples to identify features predicting benefit from the olaparib/durvalumab combination. Using GSVA analysis of RNAseq data, high levels of the Cancer Hallmark “Angiogenesis” signature in the on-olaparib biopsy were

associated with worse response to therapy (PD vs. PR/SD p-value = 0.021) and survival (OS p-value = 0.003 and PFS p-value = 0.0009) but had no predictive value in the pre-treatment biopsy (Fig. 3a; Extended Data Fig. 3a). Interestingly, olaparib treatment changed the expression levels of this signature for six of the fifteen participants, with a decrease from high to low in three good responders and an increase from low to high in two poor responders (Extended Data Fig. 1b).

Olaparib alters the immune landscape in model systems and in patient tumors, and immune contexture is a key determinant of durvalumab activity[46,47]. While clinical IHC measurements of infiltrating CD4 and CD8 T cells showed no correlation with participant outcomes (data not shown), multiple immune features in the AMTEC on-olaparib samples from our multi-omic analyses were associated with PFS, OS, and RECIST best response, including gene expression signatures, protein markers, and immune cell density (summarized in Extended Data Fig. 1b and Extended Data Table 1d).

In the bulk RNAseq data, the immune-related GSVA gene sets "IL6/JAK/STAT3 Signaling", "Activated CD8 T Cells", and "T Helper Cells" were associated with favorable OS and RECIST best response (PR/SD) in the on-olaparib biopsy only (Fig. 3b-d). "Interferon Gamma Response" and "NK/CD56dim Cells" were both associated with best response (PR/SD) in the on-olaparib biopsy, but neither signature significantly associated with survival (Extended Data Fig. 3b,c). In contrast, enriched "Cytotoxic Cells" was associated with favorable OS and RECIST best response in both the pre-treatment and the on-olaparib biopsies (Extended Data Fig. 3d).

To spatially resolve changes in immune contexture in response to olaparib, we used the protein-based mIHC and DSP assays. Elevated densities of $CD20^+$ B cells and multiple $CD8^+$ T cell states were associated with improved outcomes in mIHC from on-olaparib biopsies (Fig. 4a-b, Extended Data Fig. 4a-c,q-s). Interestingly, both naïve (TBET/EOMES/$PD\text{-}1^-$; Extended Data Fig. 4q) and exhausted (PD-1/$EOMES^+$) $CD8^+$ T cells, particularly Ki-67^+ (Extended Data Fig. 4a-c), were associated with improved outcomes. This indicates that olaparib may facilitate T cell recruitment and/or expansion.

Within the myeloid compartment, high macrophage density was associated with better OS in the on-olaparib biopsy but poor PFS in the pre-treatment biopsy (Extended Data Fig. 4f,g). This contradiction may be due to differences in $CD163^+$ myeloid populations associated with response: high infiltrating $CD163^+$ macrophages in the pre-treatment biopsy associated with shorter PFS, whereas high $CD163^-$ macrophages and $CD68^+$ $CD163^-$ monocytes in the on-olaparib biopsy associated with better clinical outcomes (Extended Data Fig. 4h-j). These results indicate that elevated $CD163^+$ myeloid subsets at baseline may be an indicator of poor outcomes, and that olaparib increases the number of $CD163^-$ myeloid cells that contribute to improved responses.

Using the DSP platform, we focused on immune markers within the tumor ($PanCK^+$) compartment, which represents immune cells proximal to malignant epithelial cells. Consistent with mIHC, elevated CD45 (immune cells) and CD3 (T cells) in the tumor compartment were associated with improved outcomes in the on-olaparib biopsy, including OS and best response (Fig. 4c,d). In addition, CD68 (myelomonocytic cells), CD56 (natural killer cells), and CD11c (dendritic cells). were all associated with improved PFS and/or OS in the on-olaparib biopsy (Extended Data Fig. 4k-n). As noted above, elevated PD-L1 in the tumor compartment was associated with better OS and RECIST best response in the pre-treatment biopsy, even though clinical IHC was not (Extended Data Fig. 4o).

Our data show that while each analysis platform revealed multiple immune cell populations or markers that predicted clinical outcomes on the AMTEC trial, these predictors varied from platform-to-platform (Extended Data Fig. 1b, Extended Data Table 1d). There are a variety of possible technical explanations for this, some of which we present in the "Discussion" below. To identify cross-platform response predictors that minimize the technical nuances of each platform, we combined the findings from the three assay platforms into a unified consensus signature, using the most predictive individual findings from each.

We first combined the response predictors from each of the three individual assay platforms into single-assay consensus immune signatures (see Methods and Extended Data Fig. 1b for response predictor inclusions). A "Positive" RNAseq consensus signature was defined as high enrichment scores in four or more immune RNA signatures (GSVA gene sets) and was significantly associated with favorable OS and RECIST best response but not PFS ("IMMUNE RNA SUMMARY"; Fig. 5a, Extended Data Fig. 5a). Similarly, a "Positive" mIHC consensus signature was defined as having six or more high mIHC cell types and was significantly associated with favorable PFS and best response as well as a trend toward OS ("IMMUNE mIHC SUMMARY"; Fig. 5b, Extended Data Fig. 5b). A "Positive" DSP consensus immune signature was defined as having four or more high Immune DSP proteins and was significantly associated with favorable PFS, OS and best response ("IMMUNE DSP SUMMARY"; Fig. 5c, Extended Data Fig 5c). Importantly, the consensus immune signatures for each of the three assay platforms was associated with improved clinical outcomes when observed in the on-olaparib biopsy but not the pre-treatment biopsy.

The consensus calls showed strong concordance from platform-to-platform: RNA vs. DSP was 76% concordant, RNA vs. mIHC 74%, and DSP vs. mIHC 83% (Extended Data Fig. 1b: compare "IMMUNE RNA SUMMARY", "IMMUNE mIHC SUMMARY", and "IMMUNE DSP SUMMARY"). This finding indicates that combining individual assay predictors within each assay platform can effectively compensate for the significant technical differences across the assays as detailed in Discussion.

Importantly, a multi-omic consensus immune signature combining all three platforms strongly predicted PFS ($p=0.003$), OS ($p=0.01$), and PR/SD ($p=0.005$) in the on-olaparib biopsy but not the pre-treatment biopsy (Fig. 5d, Extended Data Fig. 5d). Taken together, evaluation of immune contexture, particularly within the on-olaparib biopsy, provides a compelling ability to predict clinical response to combined olaparib/durvalumab.

In the analyses above, biopsies from participants with better responses and longer survival tended to have higher levels of immune-related RNA signatures, mIHC cell types, and DSP proteins than non-responders, suggesting that participant outcomes are influenced by adaptive changes in tumor-infiltrating immune cells in response to olaparib. To investigate this further, we examined changes in immune signatures in matched pairs of pre- and on-olaparib biopsies to identify statistically significant changes correlated with RECIST best response. As shown in Fig. 6 and Extended Data Fig. 6, multiple markers increased on olaparib in matched biopsy pairs from participants with favorable responses but not in those with poor responses, such as $CD4^+$ T cells (pre-treatment to on-olaparib change, $p=0.0017$ for PD vs. PR/SD), $CD8^+$ T cells ($p=0.00055$ for PD vs. PR/SD), and PD-1+ cells ($p=0.00024$ for PD vs. PR/SD). Moreover, several changes induced by olaparib in responding participants were also associated with longer survival, including exhausted $CD8^+$ T cells and $CD68^+$ $CD163^-$ monocytes from mIHC (compare Fig. 6a and

Extended Data Fig. 6a to Extended Data Fig 4b,c,j) and CD3 and CD68 from DSP (compare Fig. 6b to Fig. 4d and Extended Data Fig. 4k).

TNBC classification systems that use bulk RNAseq data to define luminal, basal, mesenchymal, and immune states have been refined to encompass basal-like immune-activated (BLIA), basal-like immune-suppressed (BLIS), luminal androgen receptor (LAR), and mesenchymal (MES) subtypes[48-51]. We have since implemented and validated the latter classification algorithm within the CLIA/CAP certified OHSU Knight Diagnostic Laboratories, adding an indeterminant (IND) category for samples with insufficient confidence to discriminate between the BLIA and BLIS subtypes.

In the AMTEC study, participants with BLIS or LAR subtypes in either the pre-treatment or the on-olaparib biopsy had significantly poorer outcomes than those with either BLIA or IND (Fig. 7a,b), with a decreased OS (on-olaparib biopsy p-val=0.001) and PFS (p-val=0.001) and a significantly likelihood of RECIST best response of PD (p-val=0.035). Tumors classified as BLIA were associated with a high likelihood of benefit. Indeed, all four BLIA participants achieved a best response of SD/PR and all three BLIS/LAR participants had PD (Fig. 7c). No MES tumors were present in the sample set.

Olaparib treatment changed the TNBC subtype for several participants, from either IND to BLIA or BLIS to IND (Extended Data Table 1a). These changes were clinically relevant, as the subtype of the on-olaparib biopsy had a higher predictive value than the pre-treatment biopsy for both survival and best response (Fig. 7a,b).

The predictive value of the TNBC subtype was tested on an independent sample set treated under the same AMTEC protocol using samples not included in the stage 1 dataset described here. In this set, the best response of 7 of 8 participants (88%) was accurately predicted by the BLIA/BLIS algorithm (data not shown). This training and test set approach demonstrates that despite the limited number of samples analyzed, TNBC subtype is a strong signature predicting benefit from olaparib/durvalumab that warrants further investigation, particularly in the on-olaparib biopsy.

A striking observation was that a subset of the highly ranked BLIA genes (centroid >0.5) was interferon-induced, with a median fold change of >2 (based on data from interferome.org; Extended Data Fig. 7a). However, while some genes in the BLIA signature were interferon inducible, classical interferon-induced genes such as IRFs and IFITs did not score among the highly ranked genes, indicating that the BLIA predictor potentially captures a novel interferon-induced gene set.

We analyzed an internal single-cell RNAseq data set from 13 breast cancer specimens to determine which kinds of cells express the genes defining the TNBC subtypes. As shown in Extended Data Fig. 7b, BLIA-associated genes were predominantly expressed in immune cells, including various subtypes of T cells, NK cells, myelomonocytic subsets, and dendritic cells. Consist with this, these genes were strongly associated with antigen presentation, T cell localization, and T cell killing. The BLIA-associated genes showed minimal expression in other cell types in the dataset, including cancer-associated fibroblasts, B cells, malignant cells, or normal epithelial cells. However, like the interferon-induced genes, classic T cell, macrophage, monocyte or dendritic cell genes were not part of the BLIA signature.

Discussion

The AMTEC trial, which included one month of olaparib monotherapy followed by combined olaparib and durvalumab, showed significant benefit for *BRCA1/2* wild type participants, with a median PFS of 5.52 months and OS of 12.88 months. Of the 15 evaluable participants, 4 (27%) achieved PR and 8 (53%) demonstrated clinical benefit. The overall PFS did not differ between participants with PR and those with SD, indicating that for this combination, the clinical benefit rate is the most important determinant of efficacy. The combination therapy in this trial was reasonably well-tolerated, with toxicity resolving through dose holds or reductions. Many, but not all, AMTEC participants demonstrated significant clinical benefit from the combination of olaparib and durvalumab. We therefore conducted a deep analysis of our multi-omic data sets to identify predictive markers that differ between responding participants and non-responders, particularly those that emerge as an adaptation mechanism in response to olaparib monotherapy.

Despite initial expectations, several markers were non-predictive of response. These include TMB; percent PD-L1 or Ki-67 positive cells by IHC; mutations in *TP53*, the HRD pathway, or the MAPK pathway; numbers of $CD4^+$ or $CD8^+$ T cells by IHC; AR levels by IHC or DSP; biopsy location; and percent tumor content. Interestingly, two participants had mutations in *B2M* that are expected to decrease class I HLA expression on the cell surface and impair antigen presentation. Loss of B2M and HLA expression has been linked to resistance to immune checkpoint blockade[52]. Despite this, both participants with *B2M* mutations benefited from treatment, with one showing evidence of constitutive NK cell activation and the other exhibiting an olaparib-induced immune response.

Using a RAD51 foci assay, we found that neither HRC nor HRD status was sufficient to predict clinical outcomes. This may be due to the limited number of participant samples definitively classified as HRC or HRD. Importantly, our method of counting RAD51 foci exclusively in G2 cells with DNA damage revealed tumors with mixed populations of HRC and HRD cells. This suggests that clinical outcomes in PARPi-treated mTNBC patients may be adversely affected by intratumoral heterogeneity in HRR competence.

PD-L1 protein levels were predictive of outcomes in our quantitative DSP assay. Although PD-L1 clinical IHC was not a statistically significant outcome predictor, higher percentages of $PD\text{-}L1^+$ tumor cells were frequently seen in participants with favorable clinical outcomes and less common in those with unfavorable outcomes, particularly in the on-olaparib biopsy. Notably, $PD\text{-}1^+$ T cells were more abundant in on-olaparib biopsies from participants with PR/SD, indicating that olaparib either remodeled immune contexture or enhanced antigenic priming in responding participants.

We found that AKT and MAPK pathway mutations and activity identified a subset of participants with limited response to the combination of olaparib and durvalumab. The predictive value was particularly strong in on-olaparib biopsies. This supports the concept that the AKT and MAPK pathways are activated as an adaptive response to PARP inhibition, which subsequently limits the efficacy of olaparib plus durvalumab. These pathways have been implicated in the response to olaparib combination therapies in other preclinical studies and clinical trials[15,26,37,45,53]. Based on these findings, we initiated a follow-on multi-arm AMTEC trial (NCT03801369), which includes olaparib combined with either a MEK inhibitor (selumetinib) or an AKT inhibitor (capivasertib). Arm allocation in this study is largely based on analysis of MAPK and AKT pathway activation in the on-olaparib biopsy, assayed in the CLIA environment using the DSP platform.

Somewhat unexpectedly, most participants with a high "Angiogenesis" RNA signature in the on-olaparib biopsy had a poor clinical response to the olaparib/durvalumab combination. This observation is consistent with an ovarian cancer study that implicated VEGFR3 expression in resistance to olaparib and durvalumab[54], as well as the clinical benefit derived from angiogenesis-targeting PARPi combinations such as olaparib plus cediranib or bevacizumab[55-57]. Our observation that this signature changed as an adaptive response to PARPi indicates that measuring angiogenesis in on-therapy biopsies may identify a population of patients more likely to benefit from the addition of an angiogenesis inhibitor, justifying the potential toxicity associated with these combinations.

Many predictive markers were associated with immune status in the on-olaparib biopsy, supporting the contention that olaparib-mediated alterations in the immune contexture contribute to the response to the olaparib and durvalumab combination. However, not all analyzed markers showed response-dependent changes with olaparib treatment (data not shown), indicating that the immune signature predictors reflect specific changes in immune contexture induced by olaparib rather than sample set differences or differential tumor heterogeneity between responders and non-responders

Interestingly, we and others have demonstrated in preclinical studies that PARPi induces STING activation, leading to subsequent interferon production[22-24,28]. In the current study, while a baseline interferon signature was associated with response, three PR/SD participants went from a low to a high "Interferon Gamma Response" RNA signature on the on-olaparib biopsy. In contrast, one PD participant went from low to high and a second went from high to low. Since interferon signals through the JAK-STAT pathway, the observed increase in the "IL6/JAK/STAT3 Signaling" RNA signature in two of the three PR/SD participants with the high interferon signature, along with the decrease in this signature in the PD participant with a low interferon signature, support the concept that activation of interferon signaling in response to olaparib could contribute to benefit from olaparib and durvalumab.

While immune indicators from the RNA, mIHC, and DSP platforms all predicted benefit from olaparib and durvalumab, each platform identified different predictive markers. This discrepancy is not surprising, as the mIHC and DSP platforms used different antibodies and the assays were sometimes run on different cores with varying degrees of tissue heterogeneity. Additionally, the mIHC platform measures antigens at the single-cell level, while DSP and RNA sequencing yield data from populations of cells within tumor-rich regions. RNA and protein levels are often poorly correlated, especially for proteins primarily regulated through post-translational modifications rather than RNA transcription[58]. Furthermore, the limited number of samples assessed and the cut-offs for positive versus negative calls, compounded by a lack of community consensus on markers used for cell type assignments, likely influenced the statistical significance of specific markers. These factors highlight the need for further refinement of predictors within each platform using additional samples.

Despite these issues, our patient-by-patient analysis of immune activation state showed high concordance across the platforms. Interestingly, CD4, CD8, and CD20 levels measured by IHC were not predictive of response (data not shown), indicating that deeper analyses, such as those performed here, are necessary to uncover predictive signals. Further, while most of the immune markers were associated with an improved outcome, total macrophages and $CD163^+$ macrophages (M2-like) were associated with a worse outcome. An association of M2-like macrophages with poor outcomes has been identified with multiple different therapies, including ICB[59].

The BLIA/BLIS algorithm for determining TNBC subtype is particularly interesting as we have moved it to the CLIA environment, allowing its use in patient selection. The first step in utilizing the algorithm is to eliminate LAR patients, and indeed, we have excluded participants who have >80% AR levels by IHC from the ongoing AMTEC trial. Importantly, BLIS or BLIA on the on-olaparib biopsy accurately predicted participant benefit. However, clinical use of this assay is confounded by the number of participants who are Indeterminant. While most participants who were Indeterminate on the on-olaparib biopsy benefited (4/6), some did not (2/6). Thus, it is necessary to develop approaches to refine the predictive value of the BLIA/BLIS algorithm.

It is important to note that the TNBC subtype (combining IND with BLIA and LAR with BLIS) is a strong predictor of benefit on the pre-therapy biopsy with p-values of 0.03 and 0.01 for PFS and OS, respectively. The predictive value of the on-olaparib biopsy was better than that of the pre-therapy biopsy, with the pre-therapy biopsy containing about 85% of the information content of the on-olaparib biopsy. Thus, a pre-therapy analysis of BLIA/BLIS, while not optimal, does provide a high predictive value for selection of patients who are likely to benefit from the olaparib and durvalumab combination, especially when an on-olaparib biopsy is unavailable.

This study has multiple limitations, the foremost being the limited number of participants. This concern will be alleviated somewhat by the ongoing AMTEC trial with a small test set to assess potential markers; however, prospective analysis of our potential predictors in future trials is necessary. Some of the assays were only completed on a subset of participants. Despite obtaining up to six cores as part of each biopsy, there was not always sufficient material and tumor content to complete the assays. Further, the DSP data were incomplete from some samples because the assay was upgraded during the trial and there was insufficient material to re-run the analysis; we only included data from the most recent version. Finally, several of the immune characterization assays were not concordant. As discussed above, there are likely multiple reasons for this that need to be resolved.

In summary, the AMTEC trial demonstrated marked activity with acceptable toxicity. Importantly, we identified a set of potential signatures that strongly predicted participant outcomes, with a subset of these markers already validated in the CLIA environment. The ongoing AMTEC trial will provide an independent test set to validate multiple potential biomarkers and to explore their utility in predicting response to additional combination therapies.

Data Availability

All data are available through the HTAN Data Portal as part of the HTAN OHSU Atlas (https://data.humantumoratlas.org/). Raw sequencing data have been deposited to dbGAP (Project phs002371.v1.p1).

Code Availability

No new tools were developed for the analyses in this study.

Acknowledgements

This project was carried out with major support from the Oregon Health & Science University (OHSU) SMMART Program, AstraZeneca, National Institutes of Health (NIH), National Cancer Institute (NCI) Human Tumor Atlas Network (HTAN) Research Center (U2CCA233280), Breast Cancer Research Foundation, and Prospect Creek Foundation. We thank all members of the SMMART Clinical Trials

Program for support with sample collection and data management. We thank the OHSU Knight Cancer Institute BioLibrary for assistance with sample management.

Author Information

Author Contributions

GBM, ZIM, and CLC conceived and designed the study. ZIM enrolled and treated participants. ALC, JMS, DB, TYO, and FO generated visualizations and figures. ALC, JMS, JYL, and DB performed data and statistical analyses. ALC developed software and pipelines for primary data processing. GBM, ALC, JMS, ZIM, NL, and JA interpreted the data. SS, KB, JL, DB, ML, TYO, MJR, FO, and BJ generated data. ALC and JMS managed data collection, cleaning, and curation. GBM, JMS, ALC, ZIM, and SKM wrote the manuscript. GBM, CLC, SKM, and LMC supervised the project. GBM acquired funding. All authors reviewed and revised the manuscript.

Ethics Declaration

Competing Interests

ZIM has received institutional grants/research support from AstraZeneca, Eli Lilly, and GSK; and received consulting fees / advisory boards from Gilead, Lilly, Merck, Novartis, AstraZeneca, and Daiichi Sankyo. NL and JA are employees of AstraZeneca and own AstraZeneca stock. LMC has received reagent support from Cell Signaling Technologies, Syndax Pharmaceuticals, Inc., ZielBio, Inc., and Hibercell, Inc.; holds sponsored research agreements with Syndax Pharmaceuticals, Hibercell, Inc., Prospect Creek Foundation, Lustgarten Foundation for Pancreatic Cancer Research, Susan G. Komen Foundation, and the National Foundation for Cancer Research; is on the Advisory Boards for Syndax Pharmaceuticals, Dispatch Pharmateuticals, Carisma Therapeutics, Inc., CytomX Therapeutics, Inc., Shasqi, Kineta, Inc., Hibercell, Inc., Cell Signaling Technologies, Inc., Alkermes, Inc., NextCure, Guardian Bio, AstraZeneca Partner of Choice Network (OHSU Site Leader), Genenta Sciences, Pio Therapeutics Pty Ltd., and Lustgarten Foundation for Pancreatic Cancer Research Therapeutics Working Group, Inc. CLC serves on the SAB for Cepheid. GBM has licensed technologies to Myriad Genetics and NanoString; is on the SAB or is a consultant to Amphista, AstraZeneca, Chrysallis Biotechnology, GSK, ImmunoMET, Ionis, Lilly, PDX Pharmaceuticals, Signalchem Lifesciences, Symphogen, Tarveda, Turbine, and Zentalis Pharmaceuticals; and has stock/options/financial interests in Catena Pharmaceuticals, ImmunoMet, SignalChem, and Tarveda.

Methods

STUDY DESIGN

AMTEC is a single arm, open-label phase II trial to assess the efficacy of olaparib in combination with durvalumab in participants with *BRCA1/2*^{wt} mTNBC (Fig. 1a). Participants with biopsy-proven mTNBC undergo a pre-treatment biopsy, followed by a 4-week induction treatment with olaparib (300 mg PO twice daily). Participants undergo a repeat on-olaparib biopsy 4 weeks (± 7 days) after starting olaparib monotherapy (i.e., Cycle 1, Day 28 ± 7 days). Following the 4-week olaparib induction treatment, durvalumab (1500 mg IV every 4 weeks) is added to olaparib. Participants are planned to receive 12 cycles of the assigned combination therapy but may continue treatment beyond 12 cycles in the absence of disease progression or unacceptable toxicity. Participants are also offered an optional repeat biopsy at the time of disease progression. Participants will be followed after removal from protocol therapy for a maximum of 1-year post-treatment.

TRIAL OVERSIGHT

All biospecimens and data were collected under the single-center, observational study Adaptive Molecular Therapy of Evolving Cancers (AMTEC), ClinicalTrials.gov identifier NCT03801369. Written informed consent was obtained from all participants prior to enrollment. The Oregon Health & Science University (OHSU) Institutional Review Board approved the trial (IRB #18504). The study adhered to the ethical principles of the Declaration of Helsinki and followed the International Council on Harmonization guidelines on Good Clinical Practice, in compliance with all applicable laws, regulatory requirements, and conditions mandated by regulatory authorities and/or institutional review boards.

PARTICIPANTS

Eligible participants must have biopsy-proven mTNBC defined as ER <10%, PR <10%, and HER2 non-amplified per ASCO/CAP guidelines[60]. Participants with ≤2 prior chemotherapy regimens in the metastatic setting were eligible. Other inclusion criteria include: ECOG PS ≤1, tumor amenable to serial biopsies, and no prior treatment with PARPi or ICB in the metastatic setting. Key exclusion criteria include active autoimmune disease requiring steroid therapy or disease-modifying agents; history of HIV; active Hepatitis B or C infection; and/or symptomatic central nervous system metastases or carcinomatous meningitis. Of the seventeen enrolled participants, two were replaced on the trial and were thus excluded from the resulting set of fifteen in the primary endpoint ORR analysis: one did not receive durvalumab due to rapid disease progression, and the other had an orthopedic procedure unrelated to trial therapy that precluded continuation of durvalumab beyond a single dose.

ENDPOINTS

The primary endpoint is to assess overall response rate (ORR), defined as complete response (CR) and partial response (PR), for the combination of olaparib and durvalumab, determined by imaging using RECISTv1.1 criteria[33]. Secondary efficacy endpoints include clinical benefit rate (CBR) defined as CR, PR, or stable disease (SD) for ≥6 months, duration of response, progression free survival (PFS), and overall survival (OS). Safety endpoints include incidence of Grade 3 or higher toxicities per Common Terminology Criteria for Adverse Events version (CTCAE) 5.0.

STATISTICAL ANALYSIS

This study follows a Simon 2-stage Minimax design[61]. The null (ICB alone) and alternative (Olaparib + Durvalumab) hypotheses are: H_0: $\pi = 0.15$ and H_a: $\pi = 0.35$. For the primary endpoint, a total sample size of 28 participants will achieve 80% power to detect the ORR difference of 0.20 using the 2-stage Minimax design, with one-sided type I error =0.05. The trial enrolled 15 evaluable participants in stage 1, defined as all individuals who received at least one dose of the combination of olaparib and durvalumab (Extended Data Fig. 1a). The trial was designed such that it would be stopped for futility if ≤2 of 15 participants respond, otherwise, the trial was to continue into stage 2 until a total of 28 participants were enrolled. All participants enrolled in stage 1 (n=15) needed to complete at least 1 post-baseline disease restaging assessment before the interim analysis could be completed. The investigational treatment was to be considered promising and worth further investigation if there were ≥8 responses among 28 participants.

SAMPLE AVAILABILITY

Pre-treatment and on-olaparib biopsies were obtained from the 15 participants evaluable for the primary endpoints. Samples were placed in appropriate preservative (FFPE or flash frozen for RPPA) within 3 minutes to preserve post-translational modification, particularly phosphoproteins (Johnson 2022). As indicated in Extended Data Fig. 1b, the success of different assays varied across samples and assay

platforms. Neither the pre-treatment nor the on-olaparib biopsy for Participant A had adequate tumor content for analysis, so Genetrails and IHC data from a biopsy obtained 90 days previously was used for analysis. The pre-therapy biopsy from Participant I had insufficient tumor content for assays other than IHC. RNAseq failed in both samples from Participants A and I. NanoString DSP was successful on most samples as it requires limited tumor content. DSP was run in several batches using multiple versions of the assay platform. Not every antibody was included from every platform version: in particular, the immune markers were included from only the two most recent platform versions. mIHC and cycIF failed in a subset of samples that became detached from the matrix, a known problem with these assay platforms[62]. RPPA requires larger amounts of materials and was only run on a subset of participant samples.

CLINICAL IMMUNOHISTOCHEMISTRY (IHC)

Tissue is formalin-fixed for ~12 h based on ASCO/CAP guidelines[60]. ER, PR, AR, HER2, and Ki-67 IHC stains were performed in the OHSU Knight Diagnostic Laboratories on formalin-fixed, paraffin-embedded tissue, using pre-diluted antibodies intended for diagnostic use in a biotin-free protocol on a Ventana Benchmark instrument. All antibodies were sourced from Roche. Staining was interpreted and scored by a pathologist. ER, PR, and AR: Antibodies include anti-ER (CONFIRM clone SP1), #790-4324; anti-PR (CONFIRM clone 1E2), #790-2223; and anti-AR (Cell Marque clone SP107), # 760-4605. ER, PR, and AR stains are considered negative if there is nuclear staining in < 10% of the tumor cells. HER2: Staining was performed with Anti-HER2/neu (PATHWAY clone 4B5), #790-2991. HER2 scoring and interpretation are per the Ventana scoring guide as expanded by the ASCO/CAP 2013 guidelines. Ki-67: Staining was performed with anti-Ki-67 (CONFIRM clone 30-9) and reported out as percent positive cells. PD-L1: Anti-PD-L1 staining was performed by PhenoPath Laboratories (Seattle, WA) using clone 22C3 pharmDx (Agilent). Positive cells were scored by Tumor Proportion Score.

NGS: GENETRAILS® COMPREHENSIVE SOLID TUMOR PANEL

Targeted DNA sequencing was conducted at the CLIA-certified and CAP-accredited OHSU Knight Diagnostic Laboratories using the GeneTrails Solid Tumor Panel assay. DNA was extracted from tumor-rich regions that were macro-dissected from FFPE tissue. Library preparation utilized custom QiaSeq chemistry (QIAGEN) with multiplexed PCR, and sequencing was performed on an Illumina NextSeq 500/550. The DNA library was created with 9,228 custom-designed primer extension assays, covering 613,343 base pairs across 125 to 225 cancer-related genes. The panel is routinely sequenced at an average read depth exceeding 2,000 to ensure highly sensitive detection of SNVs, short insertions/deletions, and copy number alterations.

PI3K-AKT pathway genes include the following genes from the GeneTrails panel: *AKT1*, *AKT2*, *PIK3CA*, *PIK3CB, PIK3R1*, or *PTEN.* RTK-MAPK pathway genes include the following genes: *HRAS*, *KRAS*, *NRAS*, *ARAF*, *BRAF*, *RAF1*, *MAP2K1*, *MAP2K2*, *MAPK1*, *EGFR*, *ERBB2*, *ERBB3*, or *MET*. HR genes include the following*: ARID1A, ATM, ATR, ATRX, BAP1, BARD1, BRCA1, BRCA2, BRIP1, CDK12, CHEK1, CHEK2, FAM175A, FANCA, FANCC, FANCD2, FANCE, FANCF, FANCG, FANCM, MRE11A, NBN, PALB2, RAD50, RAD51, RAD51B, RAD51C, RAD51D, RAD52, RAD54L*, and *RECQL.* Immune genes include the following: *B2M, CD274, HLA-A, HLA-B, HLA-C, IDO1, IDO2, IFNGR1, IFNGR2, IRF1, JAK1, JAK2*, and *PDCD1LG*. Only alterations reported to be of Strong Clinical Significance (Tier 1) or Potential Clinical Significance (Tier 2), or with gene copy number gains ≥ 7 or losses ≤ 0.5 were reported in this study.

WHOLE EXOME SEQUENCING (WES)

Preparation of DNA was described as above at the Knight Diagnostic Laboratories. Total nucleic acid from FFPE or buffy coat was sent to Tempus Labs Inc. (Tempus Labs, Inc., Chicago, IL, USA) for exome sequencing using the Tempus xE panel. Raw sequence reads were reprocessed at OHSU following the GATK Best Practices for Somatic Variant Calling. Briefly, raw sequence FASTQ reads were aligned to the UCSC GRCh37/hg19 human genome build using BWA-MEM (0.7.12, GATK, Broad Institute) [63,64], followed by marking duplicate reads (Mark Duplicates, GATK) and base recalibration (BQSR, GATK). Somatic variants were called using MuTect2 (4.0.4.0, GATK, Broad Institute) between the FFPE (tumor) and the participant's matched normal from buffy coat. A panel of normal (PON) and the gnomAD (2.0.1) [65] germline reference resource were used to filter out technical sequencing artifacts and common polymorphisms, respectively. All analysis tools were run using an OHSU Galaxy instance (v19.01) [66]. On-olaparib WES was not performed for most participants, given the short duration between biopsies.

MUTSIG3 ANALYSIS

COSMIC mutation signatures (v2) were calculated from the somatic variants (VCF) using the MutationalPatterns R package with the hg19 genome reference (BSgenome.Hsapiens.UCSC.hg19) [43,67]. The Signature 3 (MutSig3) scores were discretized into High or Low using a threshold of 40.

RNA TRANSCRIPTOME SEQUENCING

Preparation of RNA and transcriptome sequencing was performed at the Knight Diagnostic Laboratories. Total nucleic acid was extracted and purified from macrodissected, tumor-rich areas of FFPE sections. Libraries were prepared using a TruSeq RNA Access library preparation kit and sequenced on an Illumina NextSeq500/550. Approximately 100 million reads were generated per sample. Gene expression was quantified relative to Gencode v24 transcripts using Kallisto[68,69].

GENE SET VARIATION ANALYSIS (GSVA)

GSVA, a non-parametric unsupervised method to calculate gene set or pathway scores on a per-sample basis, was conducted on the RNAseq data using the GSVA package (v1.44.5) with the 1) Molecular Signatures DataBase (MSigDB) Cancer Hallmarks (v7.5.1) and 2) 16 immune cell types gene sets[70-72]. GSVA scores values were discretized into High or Low using a threshold of 0.

REVERSE PHASE PROTEIN ARRAY (RPPA)

Protein extracts from tumor samples were analyzed with a panel of 480 proteins and phosphoproteins as previously described[73,74]. To scale the protein expression values, the RPPA data from each participant sample was merged within the TCGA primary breast cancer and SMMART-program metastatic breast cancer RPPA datasets, using the replicate-based normalization method[58,75]. The protein expression values were then *z*-scored by the Median Absolute Deviation (MAD) from a Basal classified subset of TCGA samples.

RPPA PROTEIN PATHWAY SCORES

Pathway scores were calculated from RPPA data as previously described[26,58]. To determine the pathway score for each sample, all predictors associated with positive activity of the pathway were summed minus the predictors associated with pathway inhibition. The total was then divided by the numbers of predictors in the pathway. Pathway scores values were discretized into High or Low using a threshold of 0.

NANOSTRING GEOMX DIGITAL SPATIAL PROFILING (DSP)

DSP was performed by the OHSU Knight Diagnostic Laboratories. A single FFPE slide per sample was used for DSP protein panel analysis. FFPE sections (4-5 micron) were deparaffinized and subjected to antigen retrieval in Citrate buffer, pH 6.0 for 15 minutes using a pressure cooker. The slides were then incubated with a cocktail of oligonucleotide-tagged antibodies together with two fluorescent-tagged morphological markers, pan-CK (Alexa 532nm) and CD45 (Alexa 594nm) at 4°C overnight, followed by blocking for 1 hour with Buffer W. After antibody incubation, slides were washed with TBS-T and post-fixed with 10% neutral buffered formalin for 30 minutes. Following a brief wash with TBS-T, the sections were incubated with SYTO-13 (FITC 525nm) for 30 minutes and then placed on the DSP instrument for sample collection. Slides were scanned and tumor regions were identified based on nuclei staining and visualization markers.

A minimum of three regions of interest (ROIs; 660 micron diameter) were selected for each sample under the guidance of a board-certified pathologist in accordance with recommended practices[76]. ROIs were chosen with the goal of maximizing tumor cell content, avoiding any areas of necrosis or sectioning artifacts on the slide. UV-released oligonucleotide barcodes were collected automatically in a 96-well plate, then hybridized with GeoMx hyb codesets at 67°C for 16 hours and quantitated using the MAX nCounter system.

Assays were run on three versions of the assay platform: 1.1, 1.2, and 2.0. Antibodies differed among the three platform versions (see Supplementary Table 1 for antibody list), but the same analysis pipeline was used for all. A control tissue microarray was included in every run, the signals from which were used to correct for batch effects. Based on comparison with normalized signals from a 19-sample mixed breast cancer cohort, sample values were discretized with z-score percentiles above 25 as “High” for the immune proteins and AR, and above 75 as “High” for the PI3K-AKT and RTK-MAPK pathways. We considered the PI3K-AKT pathway to be activated if at least two of three pathway phosphoproteins (p-AKT1, p-GSK3B, and p-PRAS40) were above the 75th percentile. We considered the RTK-MAPK pathway to be activated if at least two of three pathway phosphoproteins (p-MEK1, p-ERK1/2, and p-p90RSK) were above the 75th percentile.

MULTIPLEX IMMUNOHISTOCHEMISTRY (mIHC)

Multiple immunohistochemistry (mIHC) was performed as previously described[77] and following (https://www.protocols.io/view/mihc-staining-ohsu-coussens-39-lab-sop-3i6gkhe). Antibody information is listed in Supplementary Table 2. Briefly, FFPE human tissues were sectioned at 5 microns and mounted on positively charged slides (Tanner Adhesive Slides, Mercedes Medical, TNR WHT45AD). Slides were baked overnight at 55 °C followed by an additional baking step for 30 minutes at 58-60 °C. They were then deparaffinized in xylene and graded ethanol (Xylene 2 x 5 min, 100% EtOH 2 x 2 min, 95% EtOH 2 x 2 min, 70% EtOH 2 x 2 min, 50% EtOH 1 x 2 min, diH2O 2 x 2 min). Slides were counterstained in Hematoxylin (Dako S3301), underwent heat-mediated antigen retrieval in pH 6.0 Citra solution (BioGenex, Fremont, CA, USA), blocked in Dako Dual Endogenous Enzyme Block (S2003, Dako, Santa Clara, CA, USA), and subjected to protein blocking with 5% normal goat serum and 2.5% bovine serum albumin (BSA) in tris-buffered saline-0.1% Tween (TBST). Slides were incubated with primary antibodies for 1 hour at room temperature or 16–17 hours at 4 °C. Primary antibody was washed off in TBST, and either anti-rat, anti-mouse, or anti-rabbit Histofine Simple Stain MAX PO horseradish peroxidase-conjugated polymer (Nichirei Biosciences, Tokyo, Japan) was applied for 30 min at room temperature, followed by AEC chromogen (Vector Laboratories, Burlingame, California, USA).

Images were acquired using the Aperio ImageScope AT (Leica Biosystems) at ×20 magnification. Following acquisition, coverslips were gently removed in 1×TBST while agitating. Removal of AEC and HRP inactivation was accomplished by incubating the slides in 0.6% fresh H_2O_2 in methanol for 15 minutes. AEC removal and stripping of antibodies was accomplished by ethanol gradient incubation and heat-mediated antigen retrieval such as described above between cycles. After washing and protein blocking, samples were subjected to the next round of staining. Some samples failed due to tissue loss during staining and image acquisition. Cell phenotypes were assigned with hierarchically gating and quantified to cell densities (cells/mm^2). Cell phenotype densities were log10 transformed and z-centered as continuous variables that were discretized as "High" for samples ≥ 0 and "Low" for < 0.

HR DETECTION ASSAY

HR efficiency was assessed by a modification of a published protocol[39,41] whereby RAD51 foci, which represent functional HR repair complexes, are assessed in cells that are both Geminin positive (G2 phase) and γH2AX foci positive (double strand DNA breaks). For IF staining of formalin-fixed, paraffin-embedded (FFPE) tissue samples, 5 µm sections were deparaffinized using xylene twice for 10 minutes, 100% ethanol twice for 10 minutes, 95% ethanol for 5 minutes, 70% ethanol for 5 minutes, and 50% ethanol for 5 minutes, and then left in PBS. Tissues were antigen retrieved in a pressure cooker using Citrate (pH 6) and DAKO antigen retrieval (pH 9) buffers. Tissues were washed twice in PBS and then were further permeabilized with 0.4% Triton X-100 in PBS for 1 hour. The excess permeabilization solution was removed by washing three times in PBS, and then a hydrophobic barrier was placed around the mounted tissue. Tissues were blocked with 3% BSA in PBS prior to antibody labeling. The tissues were then incubated with primary antibodies Rad51 (1:1500; Abcam #ab133534), Geminin (1:15, #NCL-L, Leica), and γH2AX (1:400; EMD #05-636) on a rocker for 2 hours at room temperature in a humidity chamber. After three PBS washes, secondary antibodies (1:500, Invitrogen #A21428, 1:500, Biotium #20253-1, 1:1000, Invitrogen #A21131) were applied. After three final PBS washes, all tissue samples were postfixed with 4% PFA for 10 minutes at room temperature. Hoechst staining solution (1:5000) was used and mounted in Prolong Gold Antifade mounting media. Sample images were acquired using a spinning disk confocal microscope with a 40x dry objective. Raw image files from Zen (.czi) were imported into custom ImageJ macro software for image segmentation. WEKA machine learning plugin was used for both nuclei and foci segmentation. HRC nuclei were defined as having ≥ 5 RAD51 foci, while HRD cells were defined as RAD51 negative nuclei with ≥ 3 γH2AX+ foci. The relative contributions of both HRC and HRD nuclei were used to stratify participants.

TNBC SUBTYPE CALLING

CLIA TNBC subtypes were computed using a refined list of 77 genes using a novel algorithm[48,50]. Sample gene expression was batch corrected using Removal of Unwanted Variation (RUVg)[78]. Spearman's correlation was computed between the gene expression values and each centroid. Patient samples were assigned to the centroid with the highest correlation. Calls were considered indeterminate (IND) if the difference between the top two centroids was less than 0.1. Tumors were classified as immune activated (BLIA), basal immune suppressed (BLIS), luminal androgen receptor (LAR), or mesenchymal (MES) subtypes.

IMMUNE CONSENSUS

For the RNAseq-based Immune Consensus "IMMUNE RNA SUMMARY", "Positive" is defined as having at least 4 of 6 High Immune RNA Signatures derived from the GSVA of the RNA transcriptome sequencing shown in Extended Data Fig. 1b.

For the mIHC-based Immune Consensus "IMMUNE mIHC SUMMARY", "Positive" is defined as having a predictor score of least 6 for the number of all positively associated mIHC Cell Types shown in Extended Data Fig. 1b minus the number of negatively associated mIHC Cell Types. Positively-associated mIHC cell types had a statistically significant association with a favorable best response, PFS, or OS and include "Immune Cells", "Ki-67$^+$ Immune Cells", "Ki-67$^+$ CD8$^+$ T Cells", "CD8$^+$ T Cells", "Ki-67$^+$ Exhausted CD8$^+$ T Cells", "Ki-67$^+$ TBET/EOMES/PD-1$^-$ CD8$^+$ T Cells", "PD-1$^+$ CD8$^+$ T Cells", "T regulatory CD4 Cells", "CD20$^+$ B Cells", "CCR2$^+$ Cells", "CD163$^-$ Macrophages", "CD68$^+$ CD163$^-$ Monocytes", "Other Immune Cells", and "Macrophages" (on-olaparib only). Negatively associated mIHC cell types had a statistically significant association with an unfavorable best response, PFS, or OS, and include "CD163$^+$ Macrophages" and "Macrophages" (pre-treatment only).

For the DSP-based Immune Consensus "IMMUNE DSP SUMMARY", a "Positive" summary is defined as having at least 4 of 6 High NanoString DSP Immune proteins shown in Extended Data Fig. 1b.

For the "MULTI-OMIC IMMUNE CONSENSUS", the "IMMUNE RNA SUMMARY", the "IMMUNE mIHC SUMMARY", and the "IMMUNE DSP SUMMARY" data set summaries were combined and assigned "Positive", "Negative", or "Intermediate" values using the following criteria: 1) for samples with 3 complete data sets, "Positive" is defined as having either 2 or 3 positive data set summaries and "Negative" as either 0 or 1; 2) for samples with 2 complete data sets, "Positive" is defined as having 2 positive data set summaries, "Indeterminate" as 1, and "Negative" as 0; and 3) samples with only 1 complete data set are "Indeterminate". Only "Positive" and "Negative" samples from the listed Immune Consensus summaries in Extended Data Fig. 1b were included in these analyses.

STASTICAL TESTING

Feature selection within each data type was performed using Boruta and Bonferroni multiple comparison adjustment to identify confirmed and tentative features of importance for predicting best response. Progression free survival and overall survival estimates were calculated using a Kaplan-Meier estimator with plain or log confidence intervals. Reported unadjusted p-values are indicated for both the logrank score test and Cox proportional hazards model. Comparisons of continuous datasets were performed with two-sided student's t-test; comparisons of discrete datasets were performed with Fisher's exact test.

SINGLE-CELL RNA SEQUENCING (scRNAseq)

Thirteen biospecimens were collected from participants with metastatic breast cancer under an IRB-approved MMTERT observational study[79] (OHSU IRB #16113). Fresh core needle biopsies were disaggregated using gentleMACS kits (Miltenyi Biotec, #130-095-929) following the manufacturer's instructions and filtered through a 70-µm cell strainer. Cells were collected by centrifuging (300g for 7 min at 4 °C) and resuspended at 700–1200 cells/µl. Live cells were isolated with a EasySep Dead Cell Removal (Annexin V) Kit (STEMCELL Technologies, #17899). Single cell suspensions of viable cells were processed using a Chromium Next GEM Single Cell 3' Kit v3.1 (10xGenomics) following the manufacturer's protocol. The entire mixed cell population was analyzed without sorting or enriching specific cell subtypes. Briefly, viable single cells were encapsulated into GEMs containing barcoded oligonucleotides. 5,000-10,000 GEMs were then subjected to cell lysis, reverse transcription, and cDNA

amplification. Libraries were constructed from the amplified cDNA, and sequencing was performed on the Illumina NovaSeq platform. Raw sequencing data were aligned to GRCh38 genome reference using 10X software CellRanger (Version 6.1.2) with default parameters.

To ensure high-quality data, we used Scanpy[80] to implement three quality control measures on the raw gene-cell-barcode matrix for each cell: 1) the proportion of mitochondrial genes (≤20%), 2) unique molecular identifiers (UMIs, ranging from 400 to 120,000), and 3) gene count (ranging from 200 to 10,000). Doublets were identified and removed from each sample using Scrublet[81]. Normalization of total counts per cell was performed using the normalize_total function in Scanpy, followed by log-normalization with the log1p function. Clustering was conducted using the Leiden algorithm at a resolution of 1 in Scanpy.

Marker genes for each cluster were identified using a t-test implemented in Scanpy. These marker genes were then used to annotate each cluster using publicly available databases including CellMarker[82] and PanglaoDB[83] to determine cell identities. These annotations were later refined using the CellTypist[84] package with the celltypist.annotate function. The model 'Immune_All_High.pkl' was specified, with majority voting enabled. Through this process, seven major cell type clusters were annotated: epithelial cells, natural killer cells, myeloid cells, T cells, B cells, fibroblasts, and endothelial cells. To distinguish malignant cells, we calculated and identified large-scale chromosomal copy number variation (CNV) using inferCNV[85] and CaSpER[86] tools for each sample based on transcriptomes. T cells and myeloid cells were used as reference cells, and epithelial cells with differing CNV patterns and higher CNV score were annotated as malignant cells.

Datasets were merged across different samples using SCVI[87] based integration. The top 4,000 highly variable genes were used to train the VAE models, with each biopsy as covariate key. After training the initial VAE model, the annotated cell types were used to build an extended model with scANVI[88] for better integration.

After integration, NK cells, myeloid cells, T cells, B cells, and fibroblasts were further classified using the following publicly available scRNAseq datasets: NK cells (GSE212890[89]); T cells, myeloid cells, and B cells (GSE169426[90]) and fibroblasts (GSE103322, GSE132465, GSE154778, and GSE212966[91]). The label transfer method was performed using the scArches[92] algorithm, following the best practices described previously[93].

Dot plots were generated using the Scanpy DotPlot function to visualize the expression patterns of a panel of previously defined TNBC subtype markers[50] across various cell types.

VISUALIZATIONS

Visualizations of boxplots, and bar plots, swimmer, Kaplan-Meier curves were plotted with R using ggplot2, ggpubr, and ggstatsplot, or in Python using matplotlib. The CoMut plot was generated using Python library CoMut[94].

FIGURE LEGENDS

MAIN

Table 1. Summary of clinical features of AMTEC trial participants at baseline.

Figure 1. Description of the AMTEC trial.
a) Schematic of AMTEC trial design, key eligibility criteria, timing of treatment and biopsy collections, treatment discontinuation, and post-treatment follow-up.
b) Swimmer plot of participant time on treatment (x-axis) in months for 15 trial participants A through O (see Extended Data Fig. 1a). Best response based on Response Evaluation Criteria in Solid Tumors (RECIST), version 1.1[33], is labeled adjacent to treatment duration bars. Treatment durations for participants with best response of SD or PR is in orange and PD is in purple. Participant B * = deceased from trial-unrelated accident; Participant M ** = voluntarily withdrew from study by personal choice. SD = Stable Disease; PR = Partial Response; PD = Progressive Disease.
c) Best percentage change from baseline in the sum of all target lesions for 14 trial participants. Lesions from Participant N were not evaluable. The dashed lines at 20% and −30% indicate progressive disease and partial response, respectively, based on RECIST. * = new lesions.
d) Kaplan-Meier curves of Overall Survival (left) and Progression Free Survival (right) in months for 14 trial participants, excluding Participant M (see Extended Data Fig. 1a). Median survival is indicated as dashed line. Upper and lower 95% confidence intervals are based on plain survival probability.
e) Kaplan-Meier curve of Overall Survival (left) and Progression Free Survival (right) for 14 trial participants, stratified by RECIST best response PD (purple) and PR or SD (PR/SD, orange). Median survival per strata is indicated as dashed line. P-values based on log-rank test. Upper and lower 95% confidence intervals are based on plain survival probability.

Figure 2. Tumor-intrinsic signatures of response to olaparib and durvalumab.
a) Boxplot of PAR protein levels (RPPA; y-axis) in pre-treatment (Pre-) and on-olaparib (On-) biopsies (x-axis), separated by best response PD (purple, left) and PR/SD (orange, right). P-values are based on paired Student's t-test comparison of pre-treatment vs. on-olaparib. * = p-value less than 0.05; ns = not significant.
b) Survival curve using Kaplan-Meier of Overall Survival in months, stratified by High (red) and Low (blue), for the Mutation Signature 3 (MutSig3) based on WES from the pre-treatment biopsy. Hazard Ratios (HR) and p-values for the Cox proportional hazard (CoxPH) model and Log-rank tests are labeled. Upper and lower 95% confidence intervals are based on log survival probability.
c) Survival curve using Kaplan-Meier of Overall Survival in months, stratified by presence (Positive, blue) or absence (Negative, red) of mutated or copy-number altered genes in the PI3K-AKT pathway or PI3K-AKT pathway activation by DSP or both. The pre-treatment biopsyis shown on the left and the on-olaparib biopsy is shown on the right. See Methods for gene and phosphoprotein inclusions and sequencing panel details. Hazard Ratios (HR) and p-values for the CoxPH model and Log-rank tests are labeled. Upper and lower 95% confidence intervals are based on log survival probability. Insets: Stacked bar plot of the percent of samples (y-axis) with (Positive) or without (Negative) PI3K-AKT pathway mutations (x-axis). The percent of samples from participants with best response PD are indicated in purple and PR/SD in orange. P-values are from the Fisher's exact test.
d) Survival curve using Kaplan-Meier of Overall Survival in months, stratified by presence (Positive, blue) or absence (Negative, red) of RTK-MAPK pathway activation as measured by NanoString DSP. See

Methods for phosphoprotein inclusions and pathway activation criteria. Hazard Ratios (HR) and p-values for the CoxPH model and Log-rank tests are labeled. Upper and lower 95% confidence intervals are based on log survival probability.
e) Survival curve using Kaplan-Meier of Overall Survival, stratified by presence (Positive, blue) or absence (Negative, red) of either RTK-MAPK or PI3K-AKT pathway activation as measured by NanoString DSP. Hazard Ratios (HR) and p-values for the CoxPH model and Log-rank tests are labeled. Upper and lower 95% confidence intervals are based on log survival probability. Insets: Stacked bar plot of the percent of samples (y-axis) with (Positive) or without (Negative) RTK-MAPK or PI3K-AKT pathway activation (x-axis). The percent of samples from participants with best response PD are shown in purple and PR/SD in orange. P-values are from the Fisher's exact test.

Figure 3. Microenvironment signatures of response to olaparib and durvalumab: RNA signatures. Survival curve using Kaplan-Meier of Overall Survival in months, stratified by High (red) or Low (blue) gene set enrichment of the indicated RNA signatures, in the pre-treatment (left) and on-olaparib biopsies (right). Enrichment scores (as a continuous variable) were discretized as High for scores ≥ 0 and Low for < 0. Hazard Ratios (HR) and p-values for the CoxPH model and Log-rank tests are labeled. Upper and lower 95% confidence intervals are based on log survival probability. Insets show boxplots of the gene signature enrichment score (y-axis) for samples from participants with best response (x-axis) PD are indicated in purple and PR/SD in orange for each RNA signature for the pre-treatment (left inset) and on-olaparib (right inset) biopsies. P-values from the Student's t-test are labeled: * = $p \leq 0.05$; ** = $p \leq 0.01$; ns = not significant ($p > 0.05$).
a) High vs. Low Hallmark Angiogenesis RNA signature.
b) High vs. Low Hallmark IL6/JAK/STAT3 Signaling RNA signature.
c) High vs. Low Activated CD8 T Cells RNA signature.
d) High vs. Low T Helper Cells RNA signature.

Figure 4. Microenvironment signatures of response to olaparib and durvalumab: protein signatures.
Survival curves using Kaplan-Meier of Overall Survival (OS) or Progression Free Survival (PFS) for the indicated immune cell lineages/state densities (mIHC) or protein levels (DSP) in the pre-treatment (left) and on-olaparib biopsies (right), stratified by High (red) and Low (blue). Hazard Ratios (HR) and p-values for the CoxPH model and Log-rank tests are labeled. Upper and lower 95% confidence intervals are based on log survival probability. Insets show boxplots of sample scores from participants with best response of PD (purple) and PR/SD (orange) for pre-treatment (left inset) and on-olaparib (right inset). Boxplot P-values are from the Student's t-test.
a) Progression Free Survival, High vs. Low $CD20^+$ B Cells as measured by mIHC. Scaled density of mIHC-derived immune cell lineages as continuous variables were discretized as High for samples ≥ 0 and Low for < 0.
b) Overall Survival, High vs. Low Ki-67^+ Exhausted T Cells ($CD45^+/CD3^+/EOMES^+/PD\text{-}1^+$) as measured by mIHC and scaled as in a).
c) Overall Survival, High vs. Low CD45 protein in the Tumor ($PanCK^+$) compartment as measured by NanoString DSP. Z-scored, scaled percentiles of protein levels as quantitative variables were discretized into High for samples with scaled expression $\geq$ 25th percentile or Low for $<$ 25th percentile.
d) Overall Survival, High vs. Low CD3 protein in the Tumor ($PanCK^+$) compartment as measured by NanoString DSP and scaled as in c).

Figure 5. Microenvironment signatures of response to olaparib and durvalumab: Immune Consensus signatures.
Survival curves using Kaplan-Meier of Overall Survival (OS) and Progression Free Survival (PFS) in months for the indicated Immune Consensus signatures, stratified by signature Negative (red) and Positive (blue) in the pre-treatment (left) and on-olaparib biopsies (right). Hazard Ratios (HR) and p-values for the CoxPH model and Log-rank tests are labeled. Upper and lower 95% confidence intervals are based on log survival probability. Insets show stacked bar plots of the percent of samples that are Negative or Positive for each Immune Consensus signature, with samples from participants with best response PD indicated in purple and PR/SD in orange. P-values are labeled from the Fisher's exact test. See Methods for Immune consensus design and assignment. Individual sample assignment is summarized in Extended Data Fig. 1b.
a) Overall Survival and Fisher's exact test for the RNAseq-based Immune Consensus.
b) Progression Free Survival and Fisher's exact test for the mIHC-based Immune Consensus.
c) Overall Survival and Fisher's exact test for the DSP-based Immune Consensus.
d) Overall Survival and Fisher's exact test for the Multi-Omic Immune Consensus, which combines the Immune RNA, mIHC, and DSP protein predictors.

Figure 6. Olaparib-induced response signatures and markers.
Boxplots of signature and marker changes between pre-treatment and on-olaparib biopsies for participants with a best response of PD in purple dots and PR/SD in orange. Each dot represents the difference in assay score between the on-olaparib and pre-treatment values for paired samples from the same participant, where a positive score indicates a feature was higher on the on-olaparib biopsy and a negative score indicates it was lower. Only features with statistically significant difference for paired change between paired PD and PR/SD ($p < 0.05$) based on Student's t-test are shown: * = $p <= 0.05$; ** = $p <= 0.01$; *** = $p <= 0.001$.
a) Signature changes from pre-treatment to on-olaparib for mIHC cell lineages or functional states.
b) Protein marker changes from pre-treatment to on-olaparib for DSP immune proteins in the tumor (PanCK+) compartment.
c) Signature changes from pre-treatment to on-olaparib for the Activated CD8 T Cells RNA Signature.

Figure 7. TNBC subtype correlates of response to olaparib and durvalumab.
a) and **b)** Survival curves using Kaplan-Meier of a) Overall Survival (OS) and b) Progression Free Survival (PFS) in months for RNAseq-computed TNBC subtypes, stratified by BLIS or LAR (BLIS/LAR, red) and BLIA or Indeterminate (Non-BLIS/LAR, blue) in the pre-treatment (left) and on-olaparib biopsies (right). Hazard Ratios (HR) and p-values for the CoxPH model and Log-rank tests are labeled. Upper and lower 95% confidence intervals are based on log survival probability. Insets show stacked bar plots of the percent of samples that are classified as BLIS/LAR or Non-BLIS/LAR, with the percent of samples from participants with best response of PD indicated in purple and PR/SD in orange. P-values from the Fisher's exact test are labeled.
c) Swimmer plot for 15 AMTEC trial participants showing participant time on treatment in months (x-axis) and best response RECIST (adjacent to treatment duration bars). TNBC Subtype is annotated to the left of the participant IDs, with BLIA in pink, BLIS in green, indeterminate in blue, and LAR in yellow. TNBC subtyping was performed on the on-olaparib biopsy for all participants, except for Participant A where the pre-treatment biopsy was used and Participant I where no RNA was available. * = deceased from trial-unrelated accident; ** = voluntarily withdrew from study by personal choice.

EXTENDED DATA

Table 1. Clinical summary of AMTEC trial participants.
a) Summary of clinical metadata. Data are for each biopsy from the 15 participants included in the efficacy analysis (received both study drugs and had best response determined by imaging using RECISTv1.1 criteria[33]; SD = stable disease, PR = partial response, PD = progressive disease). Progression free survival and overall survival are calculated from the beginning of the first cycle of olaparib. Percent tumor content was the fraction of tumor within pathologist-determined tumor-rich regions that were macro-dissected from FFPE tissue. TNBC subtypes were computed from RNAseq data using a list of 77 genes and classified as immune activated (BLIA), basal immune suppressed (BLIS), luminal androgen receptor (LAR), or indeterminate (IND).
b) Adverse Events. Safety analysis was performed on data from 17 participants who received at least one dose of either drug. Most treatment-related adverse events (91%) were Grades 1 or 2. Of the 38 Grade 3 or higher events, 14 (37%) were treatment-related.
c) Grades 3, 4, and 5 Adverse Events. Data are from 10 of 17 participants. The two immune-related events were resolved with a dose hold. The two Grade 5 events were unrelated to protocol therapy: one was from pain due to disease progression and one (Investigations – other*) was due to a motor vehicle accident.
d) Summary of statistically significant features correlating with response to olaparib and durvalumab, $p < 0.05$. The biopsy in which each feature was observed (pre-treatment or on-olaparib) is noted for Significant best response, Progression Free Survival (PFS), and Overall Survival (OS).

Figure 1. Description of the AMTEC trial.
a) CONSORT flow diagram for participant enrollment, exclusions, and analyses in the AMTEC trial.
b) Multi-omic clinical features and signatures from serial biopsies. Columns are sample identifiers (participant identifier appended to biopsy number), and rows are clinical or molecular signature data. White space indicates missing data. See Methods for detailed descriptions of each marker or signature. Signatures with parenthetical notations were found to be significant in one or more of the following assays: B = paired biopsy t-test; R = best response t-test; P = Kaplan-Meier analysis of Progression Free Survival (PFS); O = Kaplan-Meier analysis of Overall Survival (OS); * p-value <0.05; ** p-value < 0.005, ns = not significant.
"Best Response" is from RECIST read of tumor imaging.
"Anatomical Location" is the organ site containing the metastatic lesion from which the biopsy was obtained.
"Tumor Content" is the pathologist-estimated percent tumor content after microdissection of tumor-rich regions from FFPE slides used for GeneTrails Comprehensive Solid Tumor Panel targeted DNA sequencing.
"Ki-67 IHC", "PD-L1 IHC", and "AR IHC" were assayed by clinical IHC and defined as % positive tumor cells (Ki-67), positive or negative for tumor proportion score >1% or >10% (PD-L1), or AR positive with a cutoff of >10% AR positive tumor cells.
"PD-1^+ Cells mIHC", "PD-1^+ $CD4^+$ T Cells mIHC", "PD-$L1^+$ Cells mIHC" are mIHC-derived cell phenotypes (see Fig. 6a and MULTIPLEX IMMUNOHISTOCHEMISTRY in Methods), with scaled and z-centered values ≥0 defined as "High" and <0 as "Low".
"AR DSP" is AR protein measured within tumor cell ROIs by NanoString DSP, with z-score percentiles relative to a mixed breast cancer cohort of >25 defined as "High".
"MutSig3" is the COSMIC Mutation Signature 3, discretized into "High" or "Low" using a threshold of 40 (see also Fig. 2b)

"RPPA PAR" depicts PAR protein levels for each sample measured by RPPA, with "High" defined as a Median Absolute Deviation > 0 relative to a Basal Classified subset of TCGA samples (see also Fig. 2a).
"HRC/HRC ratio" is defined as the ratio of HRC to HRD nuclei, with ratios <15% defined as "HRD", >65% as "HRC", and in between as "Intermediate (see also Extended Data Fig. 1c-e).
"HR & Immune Genes" and "PI3K-AKT & RTK-MAPK Genes" are clinically reported by GeneTrails. Copy number gain is defined as at least 7 copies and loss is defined as less than or equal to 0.5 copies. Mutations include missense mutations, nonsense mutations, indels, and splice site substitutions. See "NGS: GENETRAILS® COMPREHENSIVE SOLID TUMOR PANEL" in Methods for pathway gene inclusions.
"Pathway Gene Alteration" for PI3K-AKT and RTK-MAPK Genes is defined as the presence of least one DNA alteration among the PI3K-AKT or the RTK-MAPK pathway genes (see also Fig. 2c and Extended Data Fig. 2a, d).
"DSP Phosphoproteins" is the level of each PI3K-AKT or RTK-MAPK pathway phosphoprotein measured within tumor cell ROIs by NanoString DSP. "High" is defined as a phosphoprotein level z-score percentile >75 relative to a mixed breast cancer cohort.
"DSP Pathway Activation" is defined as at least two of three high NanoString DSP phosphoproteins from p-AKT1, p-GSK3B, or p-PRAS40 for the PI3K-AKT DSP pathway and at least two of three high from p-MEK1, p-ERK1/2, or p-p90RSK for the RTK-MAPK DSP pathway (see also Fig. 2d-e and Extended Data Fig. 2b-c, e-k).
"Angiogenesis RNA" and the "Immune RNA Signature" gene set values were derived from GSVA scores calculated from RNA transcriptome sequencing analysis and discretized into "High" or "Low" using a threshold of zero (see also Fig. 3 and Extended Data Fig. 3).
"IMMUNE RNA SUMMARY" notes the number of Immune RNA Signatures as "High" and "Low" for each sample, with "Positive" defined as at least 4 "High" signatures (see also Fig. 5a and Extended Data Fig. 5a).
"mIHC Cell Type" is the immune cell phenotype assigned by hierarchical gating of protein co-expression and quantified to cell densities. "High" is defined as a logged and scaled z-score ≥0 and "Low" <0 (see also Fig. 4a,b and Extended Data Fig. 4a-j, p-u).
"IMMUNE mIHC SUMMARY" notes mIHC predictor score as described under "IMMUNE CONSENSUS" in Methods, with a predictor score of at least 6 (consisting of the sum of all positive predictors minus the negative predictors) defined as "Positive". See also Fig. 5b and Extended Data Fig. 5b.
"Immune DSP" notes the levels of each immune protein measured within tumor ROIs by NanoString DSP, defining z-scores >25 percentile relative a mixed breast cohort as "High" and <25 as "Low". See also Fig. 4c,d and Extended Data Fig. 4k-o.
"IMMUNE DSP SUMMARY" notes the overall DSP protein status for each sample, with "Positive" defined as at least 4 High "Immune DSP" proteins and "Low as less than 4 (see also Fig. 5c and Extended Data Fig. 5c).
"MULTI-OMIC IMMUNE CONSENSUS" notes the overall immune status in a combined three-platform signature as described in "IMMUNE CONSENSUS" in Methods. See also Fig. 5d and Extended Data Fig. 5d.
"TNBC Subtype" is described under "TNBC SUBTYPE CALLING" in Methods. See also Fig. 7a,b.
c) Representative images of Geminin, RAD51 foci, and γH2AX foci from homologous recombination deficient (HRD), intermediate, and competent (HRC) samples. RAD51 and γH2AX foci were counted in Geminin-positive nuclei. HRD nuclei were defined as having less than five RAD51 foci and more than

three γH2AX foci, and HRC nuclei were defined as having more than five RAD51 foci. Scale bar is shown as indicated.
d) Custom machine learning segmentation results from the samples shown in (c) from participants M, G, and O. Sample HR calls were defined using the ratio of HRC to HRD nuclei. HRC/HRD ratios less than 15% are defined as "Deficient", greater than 65% as "Competent", and between 15% and 65% as "Intermediate". RECIST best response is shown in orange (PR/SD) and purple (PD).
e) γH2AX positivity ratios calculated in the samples shown in (c) and represented as horizontal black bars. "Deficient" samples exhibited greater than 95% $\gamma H2AX^{+}$/$Geminin^{+}$ co-positive nuclei as highlighted in green, while "Competent" samples exhibited less than 55% as highlighted in red. The middle "Intermediate" population (blue shading) tended toward higher γH2AX positivity while having a mixture of "Competent" and "Deficient" nuclei as highlighted in blue.

Figure 2. Tumor-intrinsic signatures of response to olaparib and durvalumab.
Survival curve using Kaplan-Meier of survival probabilities, stratified by presence (Positive, blue) and absence (Negative, red) of the indicated feature in the pre-treatment (left) and on-olaparib biopsies (right). See Methods for gene and phosphoprotein inclusions and pathway activation criteria. Confidence intervals are based on plain survival probability. Insets, where present, show Fisher's exact test for absence (Negative) vs. presence (Positive) of the indicated feature for pre-treatment (left inset) and on-treatment biopsies (right inset), with percent of samples from participants with best response PD (purple) and PR/SD (orange) noted. Only statistically significant observations (p-value < 0.05) are shown.
a) Overall Survival and Fisher's exact test for Negative vs. Positive PI3K-AKT pathway gene alteration (mutation or copy number gain/loss).
b) Progression Free Survival for Negative vs. Positive PI3K-AKT pathway gene alteration (mutation or copy number gain/loss).
c) Progression Free Survival for Negative vs. Positive PI3K-AKT pathway activation as measured by DSP.
d) Progression Free Survival for Negative vs. Positive PI3K-AKT gene alteration or pathway activation.
e) Progression Free Survival for Negative vs. Positive RTK-MAPK pathway activation.
f) Progression Free Survival for Negative vs. Positive PI3K-AKT or RTK-MAPK pathway activation. Note that some samples were activated for both pathways.
g) Progression Free Survival and Fisher's exact test for Negative vs. Positive PI3K-AKT or RTK-MAPK gene alteration. No sample had gene alterations in both pathways.

Figure 3. Microenvironment signatures of response to olaparib and durvalumab: RNA signatures.
Survival curve using Kaplan-Meier of survival probabilities, stratified by High (red) and Low (blue) expression of the indicated RNA signature in the pre-treatment (left) and on-olaparib biopsies (right). Confidence intervals are based on plain survival probability. Insets, where present, show best response t-test for PD (purple) vs. PR/SD (orange) of each RNA signature for the pre-treatment (left inset) and on-treatment (right inset) biopsies.
a) Progression Free Survival for High vs. Low Angiogenesis RNA signature.
b) Overall Survival for High vs. Low Interferon Gamma Response RNA Signature. Insets show PD vs. PR/SD t-test.
c) Overall Survival for High vs. Low NK/CD56dim Cells RNA Signature. Insets show PD vs. PR/SD t-test.
d) Overall Survival for High vs. Low Cytotoxic Cells RNA Signature. Insets show PD vs. PR/SD t-test.

Figure 4. Microenvironment signatures of response to olaparib and durvalumab: protein signatures and markers.

Survival curve using Kaplan-Meier and best response t-tests for indicated proteins and protein signatures. Survival probabilities are stratified by High (red) and Low (blue) protein or protein signature expression, and confidence intervals are based on plain survival probability. T-tests compare protein expression in biopsies from participants with best response of PD (purple) vs. PR/SD (orange). Analyses of the pre-treatment biopsy are on the left and the on-olaparib biopsy are on the right. Only statistically significant observations (p-value < 0.05) are shown.

a) Progression Free Survival for High vs. Low Ki-67$^+$ Exhausted CD8$^+$ T Cells, as measured by mIHC.
b) Overall Survival for High vs. Low Exhausted CD8$^+$ T Cells, as measured by mIHC. Insets show PD vs. PR/SD t-test.
c) Progression Free Survival for High vs. Low Exhausted CD8$^+$ T Cells, as measured by mIHC.
d) Overall Survival for High vs. Low Ki-67$^+$ Immune Cells, as measured by mIHC.
e) Overall Survival for High vs. Low T Regulatory CD4$^+$ Cells, as measured by mIHC.
f) Overall Survival for High vs. Low Macrophages, as measured by mIHC.
g) Progression Free Survival for High vs. Low Macrophages, as measured by mIHC.
h) Progression Free Survival for High vs. Low CD163$^+$ Macrophages, as measured by mIHC.
i) Progression Free Survival for High vs. Low CD163$^-$ Macrophages, as measured by mIHC.
j) Progression Free Survival for High vs. Low CD68$^+$ CD163$^-$ Monocytes, as measured by mIHC. Insets show PD vs. PR/SD t-test.
k) Overall Survival for High vs. Low CD68 protein expression, as measured by NanoString DSP.
l) Progression Free Survival for High vs. Low CD68 protein expression, as measured by NanoString DSP.
m) Overall Survival for High vs. Low CD56 protein expression, as measured by NanoString DSP.
n) Progression Free Survival for High vs. Low CD11c protein expression, as measured by NanoString DSP.
o) Overall Survival for High vs. Low PD-L1 protein expression, as measured by NanoString DSP. Insets show PD vs. PR/SD t-test.
p) PD vs. PR/SD t-test for Immune Cells, as measured by mIHC.
q) PD vs. PR/SD t-test for Ki-67$^+$ TBET/EOMES/PD-1$^-$ CD8$^+$ T Cells, as measured by mIHC.
r) PD vs. PR/SD t-test for Ki-67$^+$ CD8$^+$ T Cells, as measured by mIHC.
s) PD vs. PR/SD t-test for PD-1$^+$ CD8$^+$ T Cells, as measured by mIHC.
t) PD vs. PR/SD t-test for CCR2 Cells, as measured by mIHC.
u) PD vs. PR/SD t-test for Other Immune Cells, as measured by mIHC.

Figure 5. Microenvironment signatures of response to olaparib and durvalumab: Immune Consensus signatures.

Survival curve using Kaplan-Meier of survival probabilities of Immune Consensus signatures, stratified by Negative (red) and Positive (blue) in the pre-treatment (left) and on-olaparib biopsies (right). Confidence intervals are based on plain survival probability.

a) Progression Free Survival for Immune RNA. A "Positive" summary is defined as at least 4 of 6 High RNAseq-derived Immune RNA Signatures shown in Extended Data Fig. 1b.
b) Overall Survival for Immune mIHC. See Methods for details on the quantitation of Immune mIHC Cell Types for "Positive" and "Negative" consensus categorization.
c) Progression Free Survival for Immune DSP. A "Positive" summary is defined as having at least 4 of 6 High NanoString DSP Immune proteins shown in Figure Extended Data Fig. 1b.

d) Progression Free Survival for the Multi-Omic Immune Consensus, which combines the Immune RNA, mIHC, and DSP protein data set summaries above and as shown in Extended Data Fig. 1b. For samples with 3 complete data sets, "Positive" is defined as having either 2 or 3 positive data set summaries and "Negative" as either 0 or 1. For samples with 2 complete data sets, "Positive" is defined as having 2 positive data set summaries, "Indeterminate" as 1, and "Negative" as 0. Samples with only 1 complete data set are "Indeterminate". Only "Positive" and "Negative" samples were included in these analyses.

Figure 6. Olaparib-induced response signatures and markers.
a) T-test box plots comparing mIHC Cell Type changes between pre- and on-olaparib biopsies for participants with a best response of PD (purple dots) versus PR/SD (orange dots). Each dot represents the difference in assay score between the on-olaparib and pre-treatment values for paired samples from the same participant, where a positive score indicates a feature was higher on the on-olaparib biopsy, and a negative score indicates a feature was higher on the pre-treatment biopsy. Only features with statistically significant differences for paired change between PD and PR/SD ($p < 0.05$) based on Student's t-test are shown. All features showed an increase on average in the on-olaparib biopsy in participants with a favorable response.
b) Box plots and paired t-tests comparing mIHC Cell Type scores in the pre-treatment biopsy versus on-olaparib, separated by best response of PD (purple) and PR/SD (orange). Only features with statistically significant differences between the pre-treatment and on-olaparib values in paired samples are shown. PD-1^+ Cells, PD-1^+ $CD4^+$ Cells, Ki-67^+ Exhausted $CD8^+$ T Cells, and $CD68^+$ $CD163^+$ Monocytes all increased on olaparib in samples from participants with a favorable response, while Ki-67^+ TBET/EOMES/PD-1^- $CD8^+$ T Cells decreased on olaparib in samples from participants with an unfavorable response.
c) Box plots and paired t-tests comparing DSP Immune Protein levels in pre-treatment versus on-treatment biopsies, separated by best response of PD (purple) and PR/SD (orange). Only features with statistically significant differences between the pre-treatment and on-treatment values in paired samples are shown.

Figure 7. TNBC subtype correlates of response to olaparib and durvalumab.
a) Interferon regulated genes associated with the BLIA TNBC subtype. The Interferome web tool, a database of genes regulated by interferons (http://www.interferome.org), was used to identify a subset of highly ranked, interferon-inducible genes (median Interferome gene change >2, dashed lines, Y-axis) associated with the BLIA subtype (>0.5, X-axis).
b) Dot plot visualizing expression of representative marker genes (x-axis, bottom) within TNBC subtypes (x-axis, top) and across distinct cell type clusters (y-axis). Data are from a single-cell RNA sequencing breast cancer dataset. Relative gene expression levels are represented by the color scale, and the fraction of cells within each cell type group expressing the gene is represented by the dot size. The plot highlights the differential expression patterns of key TNBC markers within each cell cluster, providing insights into the heterogeneity and distribution of TNBC-related gene expression profiles at the single-cell level.

References

1 Foulkes, W. D., Smith, I. E. & Reis-Filho, J. S. Triple-negative breast cancer. *N Engl J Med* **363**, 1938-1948 (2010). https://doi.org:10.1056/NEJMra1001389

2 Bardia, A. *et al.* Sacituzumab Govitecan in Metastatic Triple-Negative Breast Cancer. *N Engl J Med* **384**, 1529-1541 (2021). https://doi.org:10.1056/NEJMoa2028485

3 Cortés, J. *et al.* LBA16 KEYNOTE-355: Final results from a randomized, double-blind phase III study of first-line pembrolizumab + chemotherapy vs placebo + chemotherapy for metastatic TNBC. *Annals of Oncology* **32**, S1289-S1290 (2021). https://doi.org:10.1016/j.annonc.2021.08.2089

4 Modi, S. *et al.* Trastuzumab deruxtecan (T-DXd) versus treatment of physician's choice (TPC) in patients (pts) with HER2-low unresectable and/or metastatic breast cancer (mBC): Results of DESTINY-Breast04, a randomized, phase 3 study. *Journal of Clinical Oncology* **40**, LBA3-LBA3 (2022). https://doi.org:10.1200/JCO.2022.40.17_suppl.LBA3

5 Glodzik, D. *et al.* Comprehensive molecular comparison of BRCA1 hypermethylated and BRCA1 mutated triple negative breast cancers. *Nat Commun* **11**, 3747 (2020). https://doi.org:10.1038/s41467-020-17537-2

6 Shimelis, H. *et al.* Triple-Negative Breast Cancer Risk Genes Identified by Multigene Hereditary Cancer Panel Testing. *J Natl Cancer Inst* **110**, 855-862 (2018). https://doi.org:10.1093/jnci/djy106

7 Winter, C. *et al.* Targeted sequencing of BRCA1 and BRCA2 across a large unselected breast cancer cohort suggests that one-third of mutations are somatic. *Ann Oncol* **27**, 1532-1538 (2016). https://doi.org:10.1093/annonc/mdw209

8 Morganti, S. *et al.* PARP Inhibitors for Breast Cancer Treatment: A Review. *JAMA Oncol* **10**, 658-670 (2024). https://doi.org:10.1001/jamaoncol.2023.7322

9 Litton, J. K. *et al.* Talazoparib in Patients with Advanced Breast Cancer and a Germline BRCA Mutation. *N Engl J Med* **379**, 753-763 (2018). https://doi.org:10.1056/NEJMoa1802905

10 Robson, M. *et al.* Olaparib for Metastatic Breast Cancer in Patients with a Germline BRCA Mutation. *N Engl J Med* **377**, 523-533 (2017). https://doi.org:10.1056/NEJMoa1706450

11 Lynce, F. & Robson, M. Clinical Use of PARP Inhibitors in BRCA Mutant and Non-BRCA Mutant Breast Cancer. *Cancer Treat Res* **186**, 91-102 (2023). https://doi.org:10.1007/978-3-031-30065-3_6

12 Tutt, A. *et al.* 161O VIOLETTE: Randomised phase II study of olaparib (ola) + ceralasertib (cer) or adavosertib (ada) vs ola alone in patients (pts) with metastatic triple-negative breast cancer (mTNBC). *Annals of Oncology* **33**, S194-S195 (2022). https://doi.org:10.1016/j.annonc.2022.03.180

13 Konstantinopoulos, P. A. *et al.* Single-Arm Phases 1 and 2 Trial of Niraparib in Combination With Pembrolizumab in Patients With Recurrent Platinum-Resistant Ovarian Carcinoma. *JAMA Oncol* **5**, 1141-1149 (2019). https://doi.org:10.1001/jamaoncol.2019.1048

14 Labrie, M. *et al.* Multiomics analysis of serial PARP inhibitor treated metastatic TNBC inform on rational combination therapies. *NPJ Precis Oncol* **5**, 92 (2021). https://doi.org:10.1038/s41698-021-00232-w

15 Westin, S. N. *et al.* Phase Ib Dose Expansion and Translational Analyses of Olaparib in Combination with Capivasertib in Recurrent Endometrial, Triple-Negative Breast, and Ovarian Cancer. *Clin Cancer Res* **27**, 6354-6365 (2021). https://doi.org:10.1158/1078-0432.CCR-21-1656

16 Morad, G., Helmink, B. A., Sharma, P. & Wargo, J. A. Hallmarks of response, resistance, and toxicity to immune checkpoint blockade. *Cell* **184**, 5309-5337 (2021). https://doi.org:10.1016/j.cell.2021.09.020

17 Sun, Q. *et al.* Immune checkpoint therapy for solid tumours: clinical dilemmas and future trends. *Signal Transduct Target Ther* **8**, 320 (2023). https://doi.org:10.1038/s41392-023-01522-4

18 Cortes, J. *et al.* Pembrolizumab plus Chemotherapy in Advanced Triple-Negative Breast Cancer. *N Engl J Med* **387**, 217-226 (2022). https://doi.org:10.1056/NEJMoa2202809

19 Haricharan, S., Bainbridge, M. N., Scheet, P. & Brown, P. H. Somatic mutation load of estrogen receptor-positive breast tumors predicts overall survival: an analysis of genome sequence data. *Breast Cancer Res Treat* **146**, 211-220 (2014). https://doi.org:10.1007/s10549-014-2991-x

20 Fang, Y. *et al.* Sequential Therapy with PARP and WEE1 Inhibitors Minimizes Toxicity while Maintaining Efficacy. *Cancer Cell* **35**, 851-867 e857 (2019). https://doi.org:10.1016/j.ccell.2019.05.001

21 Huang, J. *et al.* The PARP1 inhibitor BMN 673 exhibits immunoregulatory effects in a Brca1(-/-) murine model of ovarian cancer. *Biochem Biophys Res Commun* **463**, 551-556 (2015). https://doi.org:10.1016/j.bbrc.2015.05.083

22 Pantelidou, C. *et al.* PARP Inhibitor Efficacy Depends on CD8(+) T-cell Recruitment via Intratumoral STING Pathway Activation in BRCA-Deficient Models of Triple-Negative Breast Cancer. *Cancer Discov* **9**, 722-737 (2019). https://doi.org:10.1158/2159-8290.CD-18-1218

23 Shen, J. *et al.* PARPi Triggers the STING-Dependent Immune Response and Enhances the Therapeutic Efficacy of Immune Checkpoint Blockade Independent of BRCAness. *Cancer Res* **79**, 311-319 (2019). https://doi.org:10.1158/0008-5472.CAN-18-1003

24 Wang, Z. *et al.* Niraparib activates interferon signaling and potentiates anti-PD-1 antibody efficacy in tumor models. *Sci Rep* **9**, 1853 (2019). https://doi.org:10.1038/s41598-019-38534-6

25 Farkkila, A. *et al.* Immunogenomic profiling determines responses to combined PARP and PD-1 inhibition in ovarian cancer. *Nat Commun* **11**, 1459 (2020). https://doi.org:10.1038/s41467-020-15315-8

26 Labrie, M. *et al.* Adaptive responses in a PARP inhibitor window of opportunity trial illustrate limited functional interlesional heterogeneity and potential combination therapy options. *Oncotarget* **10**, 3533-3546 (2019). https://doi.org:10.18632/oncotarget.26947

27 Labrie, M., Brugge, J. S., Mills, G. B. & Zervantonakis, I. K. Therapy resistance: opportunities created by adaptive responses to targeted therapies in cancer. *Nat Rev Cancer* **22**, 323-339 (2022). https://doi.org:10.1038/s41568-022-00454-5

28 Ding, L. *et al.* PARP Inhibition Elicits STING-Dependent Antitumor Immunity in Brca1-Deficient Ovarian Cancer. *Cell Rep* **25**, 2972-2980 e2975 (2018). https://doi.org:10.1016/j.celrep.2018.11.054

29 Domchek, S. M. *et al.* Olaparib and durvalumab in patients with germline BRCA-mutated metastatic breast cancer (MEDIOLA): an open-label, multicentre, phase 1/2, basket study. *Lancet Oncol* **21**, 1155-1164 (2020). https://doi.org:10.1016/S1470-2045(20)30324-7

30 Vinayak, S. *et al.* Open-label Clinical Trial of Niraparib Combined With Pembrolizumab for Treatment of Advanced or Metastatic Triple-Negative Breast Cancer. *JAMA Oncol* **5**, 1132-1140 (2019). https://doi.org:10.1001/jamaoncol.2019.1029

31 Yap, T. A. *et al.* Avelumab Plus Talazoparib in Patients With Advanced Solid Tumors: The JAVELIN PARP Medley Nonrandomized Controlled Trial. *JAMA Oncol* **9**, 40-50 (2023). https://doi.org:10.1001/jamaoncol.2022.5228

32 Mitri, Z. I. *et al.* Abstract CT203: Multi-omic analysis of serial biopsies to inform biomarkers of sensitivity to olaparib and durvalumab in patients with metastatic BRCA-wildtype triple negative breast cancer (mTNBC). *Cancer Research* **84**, CT203-CT203 (2024). https://doi.org:10.1158/1538-7445.Am2024-ct203

33 Eisenhauer, E. A. *et al.* New response evaluation criteria in solid tumours: revised RECIST guideline (version 1.1). *Eur J Cancer* **45**, 228-247 (2009). https://doi.org:10.1016/j.ejca.2008.10.026

34 Chebib, I. & Mino-Kenudson, M. PD-L1 immunohistochemistry: Clones, cutoffs, and controversies. *APMIS* **130**, 295-313 (2022). https://doi.org:10.1111/apm.13223

35 Cortes, J. *et al.* Pembrolizumab plus chemotherapy versus placebo plus chemotherapy for previously untreated locally recurrent inoperable or metastatic triple-negative breast cancer (KEYNOTE-355): a randomised, placebo-controlled, double-blind, phase 3 clinical trial. *Lancet* **396**, 1817-1828 (2020). https://doi.org:10.1016/S0140-6736(20)32531-9

36 Schmid, P. *et al.* Atezolizumab and Nab-Paclitaxel in Advanced Triple-Negative Breast Cancer. *N Engl J Med* **379**, 2108-2121 (2018). https://doi.org:10.1056/NEJMoa1809615

37 Swisher, E. M. *et al.* Rucaparib in relapsed, platinum-sensitive high-grade ovarian carcinoma (ARIEL2 Part 1): an international, multicentre, open-label, phase 2 trial. *Lancet Oncol* **18**, 75-87 (2017). https://doi.org:10.1016/S1470-2045(16)30559-9

38 Tung, N. M. *et al.* TBCRC 048: Phase II Study of Olaparib for Metastatic Breast Cancer and Mutations in Homologous Recombination-Related Genes. *J Clin Oncol* **38**, 4274-4282 (2020). https://doi.org:10.1200/JCO.20.02151

39 Castroviejo-Bermejo, M. *et al.* A RAD51 assay feasible in routine tumor samples calls PARP inhibitor response beyond BRCA mutation. *EMBO Mol Med* **10** (2018). https://doi.org:10.15252/emmm.201809172

40 Eikesdal, H. P. *et al.* Olaparib monotherapy as primary treatment in unselected triple negative breast cancer. *Ann Oncol* **32**, 240-249 (2021). https://doi.org:10.1016/j.annonc.2020.11.009

41 Miller, R. E. *et al.* ESMO recommendations on predictive biomarker testing for homologous recombination deficiency and PARP inhibitor benefit in ovarian cancer. *Ann Oncol* **31**, 1606-1622 (2020). https://doi.org:10.1016/j.annonc.2020.08.2102

42 Ring, A. *et al.* Olaparib and Ceralasertib (AZD6738) in Patients with Triple-Negative Advanced Breast Cancer: Results from Cohort E of the plasmaMATCH Trial (CRUK/15/010). *Clin Cancer Res* **29**, 4751-4759 (2023). https://doi.org:10.1158/1078-0432.CCR-23-1696

43 Alexandrov, L. B. *et al.* Signatures of mutational processes in human cancer. *Nature* **500**, 415-421 (2013). https://doi.org:10.1038/nature12477

44 Sun, C. *et al.* Rational combination therapy with PARP and MEK inhibitors capitalizes on therapeutic liabilities in RAS mutant cancers. *Sci Transl Med* **9** (2017). https://doi.org:10.1126/scitranslmed.aal5148

45 Yang, B. *et al.* MEK Inhibition Remodels the Immune Landscape of Mutant KRAS Tumors to Overcome Resistance to PARP and Immune Checkpoint Inhibitors. *Cancer Res* **81**, 2714-2729 (2021). https://doi.org:10.1158/0008-5472.CAN-20-2370

46 Althammer, S. *et al.* Automated image analysis of NSCLC biopsies to predict response to anti-PD-L1 therapy. *J Immunother Cancer* **7**, 121 (2019). https://doi.org:10.1186/s40425-019-0589-x

47 Hansen, A. M. *et al.* Abstract 5466: Functional status of tumor-associated macrophages impacts clinical outcome of durvalumab in patients with advanced NSCLC as revealed by proteomics mass spectrometry. *Cancer Research* **83**, 5466-5466 (2023). https://doi.org:10.1158/1538-7445.Am2023-5466

48 Burstein, M. D. *et al.* Comprehensive genomic analysis identifies novel subtypes and targets of triple-negative breast cancer. *Clin Cancer Res* **21**, 1688-1698 (2015). https://doi.org:10.1158/1078-0432.CCR-14-0432

49 Chen, X. *et al.* TNBCtype: A Subtyping Tool for Triple-Negative Breast Cancer. *Cancer Inform* **11**, 147-156 (2012). https://doi.org:10.4137/CIN.S9983

50 Ding, Y. C. *et al.* Molecular subtypes of triple-negative breast cancer in women of different race and ethnicity. *Oncotarget* **10**, 198-208 (2019). https://doi.org:10.18632/oncotarget.26559

51 Lehmann, B. D. *et al.* Identification of human triple-negative breast cancer subtypes and preclinical models for selection of targeted therapies. *J Clin Invest* **121**, 2750-2767 (2011). https://doi.org:10.1172/JCI45014

52 Russell, B. L., Sooklal, S. A., Malindisa, S. T., Daka, L. J. & Ntwasa, M. The Tumor Microenvironment Factors That Promote Resistance to Immune Checkpoint Blockade Therapy. *Front Oncol* **11**, 641428 (2021). https://doi.org:10.3389/fonc.2021.641428

53 Batalini, F. *et al.* Phase 1b Clinical Trial with Alpelisib plus Olaparib for Patients with Advanced Triple-Negative Breast Cancer. *Clin Cancer Res* **28**, 1493-1499 (2022). https://doi.org:10.1158/1078-0432.CCR-21-3045

54 Lampert, E. J. *et al.* Combination of PARP Inhibitor Olaparib, and PD-L1 Inhibitor Durvalumab, in Recurrent Ovarian Cancer: a Proof-of-Concept Phase II Study. *Clin Cancer Res* **26**, 4268-4279 (2020). https://doi.org:10.1158/1078-0432.CCR-20-0056

55 Kim, Y. N. *et al.* Randomized, two-arm, noncomparative phase 2 study of olaparib plus cediranib or durvalumab in HRR-mutated, platinum-resistant ovarian cancer: A substudy of KGOG 3045. *Int J Cancer* **153**, 2032-2044 (2023). https://doi.org:10.1002/ijc.34696

56 Ray-Coquard, I. *et al.* Olaparib plus Bevacizumab as First-Line Maintenance in Ovarian Cancer. *N Engl J Med* **381**, 2416-2428 (2019). https://doi.org:10.1056/NEJMoa1911361

57 Zimmer, A. S. *et al.* A phase I study of the PD-L1 inhibitor, durvalumab, in combination with a PARP inhibitor, olaparib, and a VEGFR1-3 inhibitor, cediranib, in recurrent women's cancers with biomarker analyses. *J Immunother Cancer* **7**, 197 (2019). https://doi.org:10.1186/s40425-019-0680-3

58 Akbani, R. *et al.* A pan-cancer proteomic perspective on The Cancer Genome Atlas. *Nat Commun* **5**, 3887 (2014). https://doi.org:10.1038/ncomms4887

59 Wang, S. *et al.* Targeting M2-like tumor-associated macrophages is a potential therapeutic approach to overcome antitumor drug resistance. *NPJ Precis Oncol* **8**, 31 (2024). https://doi.org:10.1038/s41698-024-00522-z

60 Allison, K. H. *et al.* Estrogen and Progesterone Receptor Testing in Breast Cancer: ASCO/CAP Guideline Update. *J Clin Oncol* **38**, 1346-1366 (2020). https://doi.org:10.1200/JCO.19.02309

61 Simon, R. Optimal two-stage designs for phase II clinical trials. *Control Clin Trials* **10**, 1-10 (1989). https://doi.org:10.1016/0197-2456(89)90015-9

62 Gambella, A. *et al.* Section detachment in immunohistochemistry: causes, troubleshooting, and problem-solving. *Histochem Cell Biol* **148**, 95-101 (2017). https://doi.org:10.1007/s00418-017-1558-4

63 Li, H. & Durbin, R. Fast and accurate long-read alignment with Burrows-Wheeler transform. *Bioinformatics* **26**, 589-595 (2010). https://doi.org:10.1093/bioinformatics/btp698

64 McKenna, A. *et al.* The Genome Analysis Toolkit: a MapReduce framework for analyzing next-generation DNA sequencing data. *Genome Res* **20**, 1297-1303 (2010). https://doi.org:10.1101/gr.107524.110

65 Karczewski, K. J. *et al.* The mutational constraint spectrum quantified from variation in 141,456 humans. *Nature* **581**, 434-443 (2020). https://doi.org:10.1038/s41586-020-2308-7

66 Afgan, E. *et al.* The Galaxy platform for accessible, reproducible and collaborative biomedical analyses: 2018 update. *Nucleic Acids Res* **46**, W537-W544 (2018). https://doi.org:10.1093/nar/gky379

67 Manders, F. *et al.* MutationalPatterns: the one stop shop for the analysis of mutational processes. *BMC Genomics* **23**, 134 (2022). https://doi.org:10.1186/s12864-022-08357-3

68 Bray, N. L., Pimentel, H., Melsted, P. & Pachter, L. Near-optimal probabilistic RNA-seq quantification. *Nat Biotechnol* **34**, 525-527 (2016). https://doi.org:10.1038/nbt.3519

69 Frankish, A. *et al.* Gencode 2021. *Nucleic Acids Res* **49**, D916-D923 (2021). https://doi.org:10.1093/nar/gkaa1087

70 Hanzelmann, S., Castelo, R. & Guinney, J. GSVA: gene set variation analysis for microarray and RNA-seq data. *BMC Bioinformatics* **14**, 7 (2013). https://doi.org:10.1186/1471-2105-14-7

71 Liberzon, A. *et al.* The Molecular Signatures Database (MSigDB) hallmark gene set collection. *Cell Syst* **1**, 417-425 (2015). https://doi.org:10.1016/j.cels.2015.12.004

72 Tamborero, D. *et al.* A Pan-cancer Landscape of Interactions between Solid Tumors and Infiltrating Immune Cell Populations. *Clin Cancer Res* **24**, 3717-3728 (2018). https://doi.org:10.1158/1078-0432.Ccr-17-3509

73 Labrie, M. *et al.* Exploration of markers of synergistic lethality of PARP and PI3K-akt-mTOR inhibitors in women's cancers. *Gynecologic Oncology* **154**, 60 (2019). https://doi.org:https://doi.org/10.1016/j.ygyno.2019.04.143

74 Tibes, R. *et al.* Reverse phase protein array: validation of a novel proteomic technology and utility for analysis of primary leukemia specimens and hematopoietic stem cells. *Mol Cancer Ther* **5**, 2512-2521 (2006). https://doi.org:10.1158/1535-7163.Mct-06-0334

75 Shehwana, H. *et al.* RPPA SPACE: an R package for normalization and quantitation of Reverse-Phase Protein Array data. *Bioinformatics* **38**, 5131-5133 (2022). https://doi.org:10.1093/bioinformatics/btac665

76 Bergholtz, H. *et al.* Best Practices for Spatial Profiling for Breast Cancer Research with the GeoMx((R)) Digital Spatial Profiler. *Cancers (Basel)* **13** (2021). https://doi.org:10.3390/cancers13174456

77 Banik, G. *et al.* High-dimensional multiplexed immunohistochemical characterization of immune contexture in human cancers. *Methods Enzymol* **635**, 1-20 (2020). https://doi.org:10.1016/bs.mie.2019.05.039

78 Risso, D., Ngai, J., Speed, T. P. & Dudoit, S. Normalization of RNA-seq data using factor analysis of control genes or samples. *Nat Biotechnol* **32**, 896-902 (2014). https://doi.org:10.1038/nbt.2931

79 Mitri, Z. I. *et al.* Implementing a comprehensive translational oncology platform: from molecular testing to actionability. *J Transl Med* **16**, 358 (2018). https://doi.org:10.1186/s12967-018-1733-y

80 Wolf, F. A., Angerer, P. & Theis, F. J. SCANPY: large-scale single-cell gene expression data analysis. *Genome Biol* **19**, 15 (2018). https://doi.org:10.1186/s13059-017-1382-0

81 Wolock, S. L., Lopez, R. & Klein, A. M. Scrublet: Computational Identification of Cell Doublets in Single-Cell Transcriptomic Data. *Cell Syst* **8**, 281-291 e289 (2019). https://doi.org:10.1016/j.cels.2018.11.005

82 Hu, C. *et al.* CellMarker 2.0: an updated database of manually curated cell markers in human/mouse and web tools based on scRNA-seq data. *Nucleic Acids Res* **51**, D870-D876 (2023). https://doi.org:10.1093/nar/gkac947

83 Franzen, O., Gan, L. M. & Bjorkegren, J. L. M. PanglaoDB: a web server for exploration of mouse and human single-cell RNA sequencing data. *Database (Oxford)* **2019** (2019). https://doi.org:10.1093/database/baz046

84 Xu, C. *et al.* Automatic cell-type harmonization and integration across Human Cell Atlas datasets. *Cell* **186**, 5876-5891 e5820 (2023). https://doi.org:10.1016/j.cell.2023.11.026

85 Tickle, T., Tirosh, I., Georgescu, C., Brown, M. & Haas, B. (Cambridge, MA, 2019).

86 Serin Harmanci, A., Harmanci, A. O. & Zhou, X. CaSpER identifies and visualizes CNV events by integrative analysis of single-cell or bulk RNA-sequencing data. *Nat Commun* **11**, 89 (2020). https://doi.org:10.1038/s41467-019-13779-x

87 Gayoso, A. *et al.* A Python library for probabilistic analysis of single-cell omics data. *Nat Biotechnol* **40**, 163-166 (2022). https://doi.org:10.1038/s41587-021-01206-w

88 Xu, C. *et al.* Probabilistic harmonization and annotation of single-cell transcriptomics data with deep generative models. *Mol Syst Biol* **17**, e9620 (2021). https://doi.org:10.15252/msb.20209620

89 Tang, F. *et al.* A pan-cancer single-cell panorama of human natural killer cells. *Cell* **186**, 4235-4251 e4220 (2023). https://doi.org:10.1016/j.cell.2023.07.034

90 Dussiau, C. *et al.* Hematopoietic differentiation is characterized by a transient peak of entropy at a single-cell level. *BMC Biol* **20**, 60 (2022). https://doi.org:10.1186/s12915-022-01264-9

91 Cords, L. *et al.* Cancer-associated fibroblast classification in single-cell and spatial proteomics data. *Nat Commun* **14**, 4294 (2023). https://doi.org:10.1038/s41467-023-39762-1

92 Lotfollahi, M. *et al.* Mapping single-cell data to reference atlases by transfer learning. *Nat Biotechnol* **40**, 121-130 (2022). https://doi.org:10.1038/s41587-021-01001-7

93 Heumos, L. *et al.* Best practices for single-cell analysis across modalities. *Nat Rev Genet* **24**, 550-572 (2023). https://doi.org:10.1038/s41576-023-00586-w

94 Crowdis, J., He, M. X., Reardon, B. & Van Allen, E. M. CoMut: visualizing integrated molecular information with comutation plots. *Bioinformatics* **36**, 4348-4349 (2020). https://doi.org:10.1093/bioinformatics/btaa554

Table 1

		N = 17 (%)
Median Age (Range)	48.9 (25.3 – 78.9) years	
ECOG performance status	0	11 (65%)
	1	6 (35%)
Race	Caucasian	16 (94%)
	African American	1 (6%)
Menopausal status	Pre-menopausal	7 (41%)
	Post-menopausal	10 (59%)
Lines of therapy in the metastatic setting	0	6 (35%)
	1	6 (35%)
	2	5 (30%)
Prior platinum chemo in the metastatic setting	Yes	7 (41%)
	No	10 (59%)
History of brain metastases	Yes	4 (24%)
	No	13 (76%)

Figure 1

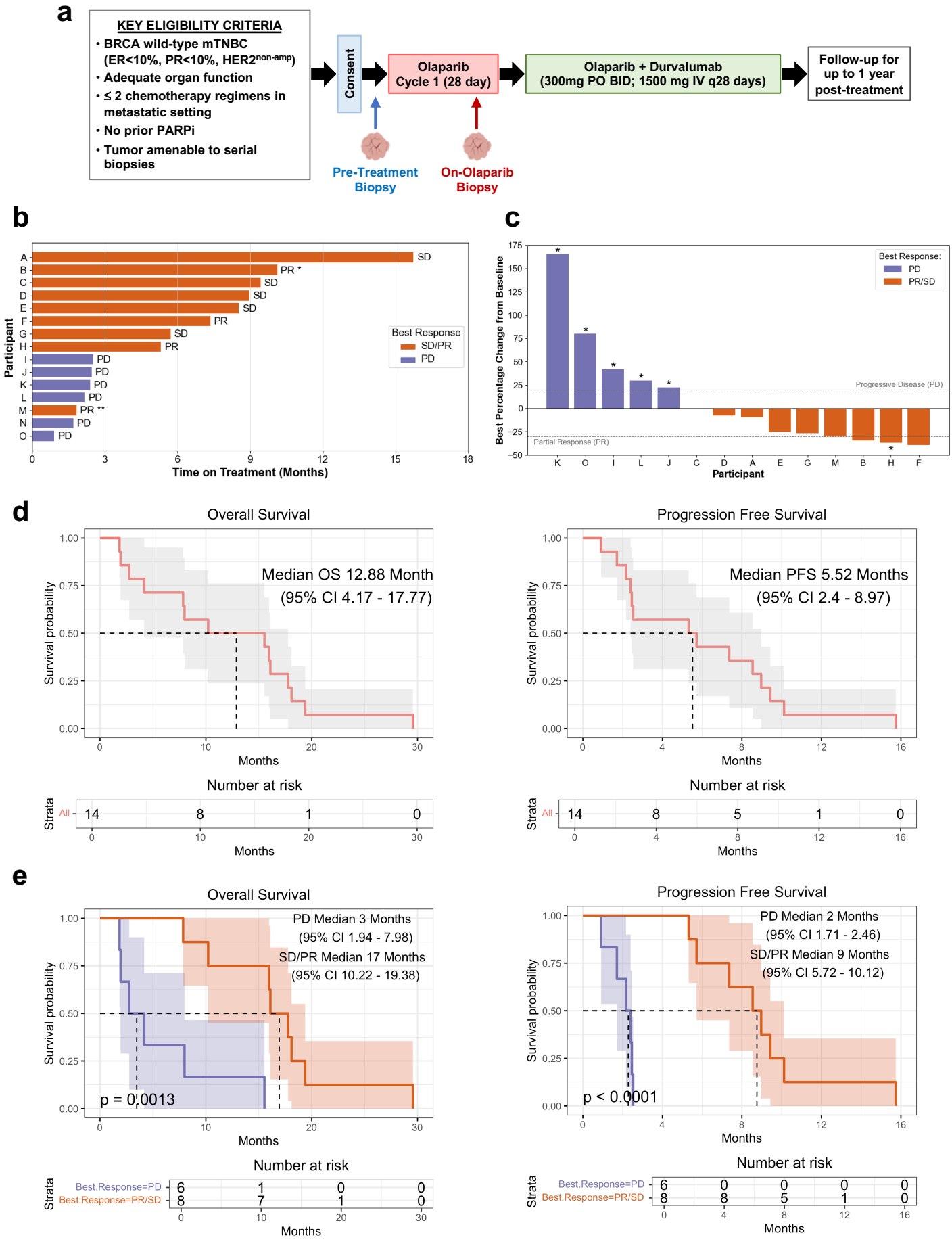

Figure 2

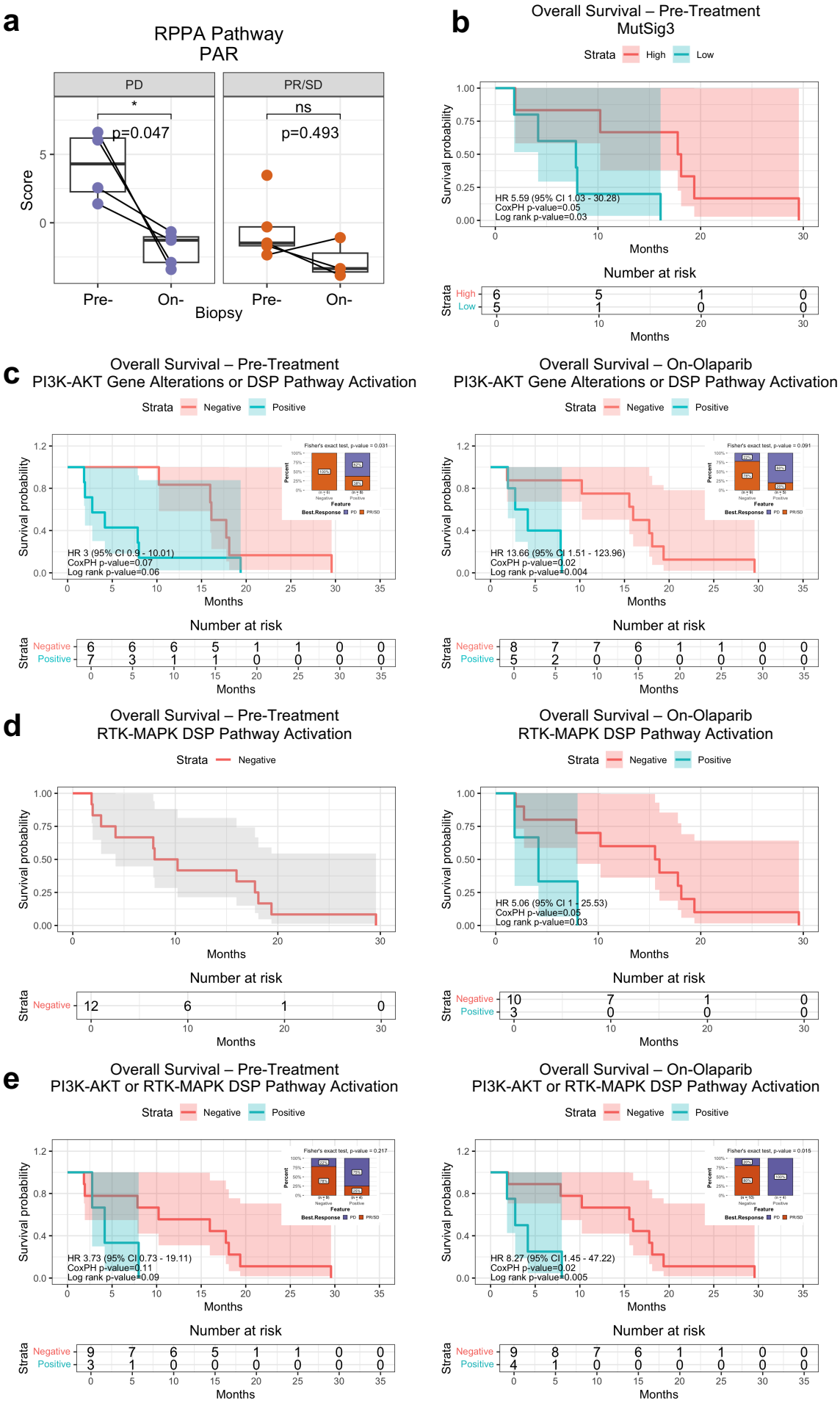

Figure 3

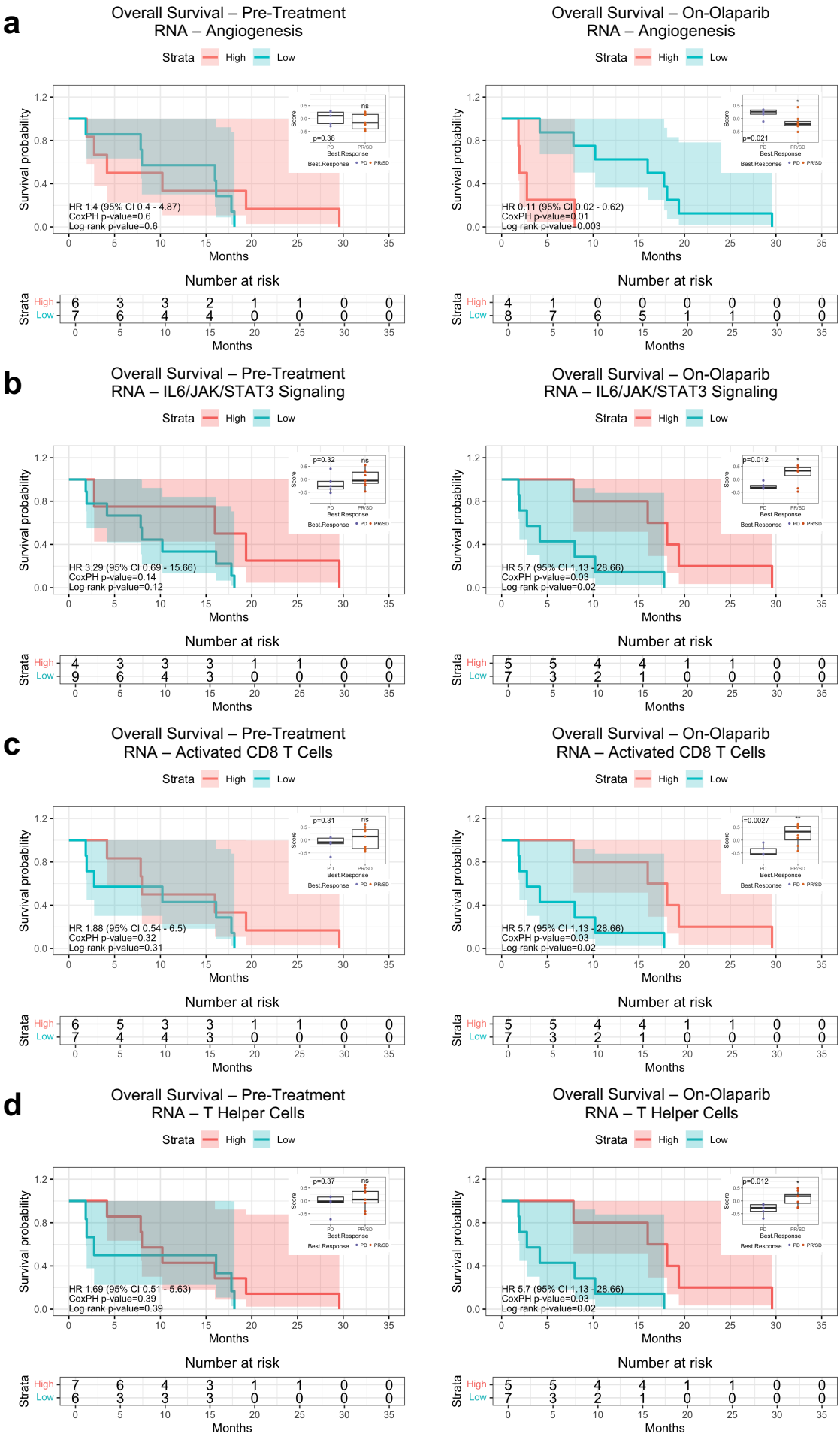

Figure 4

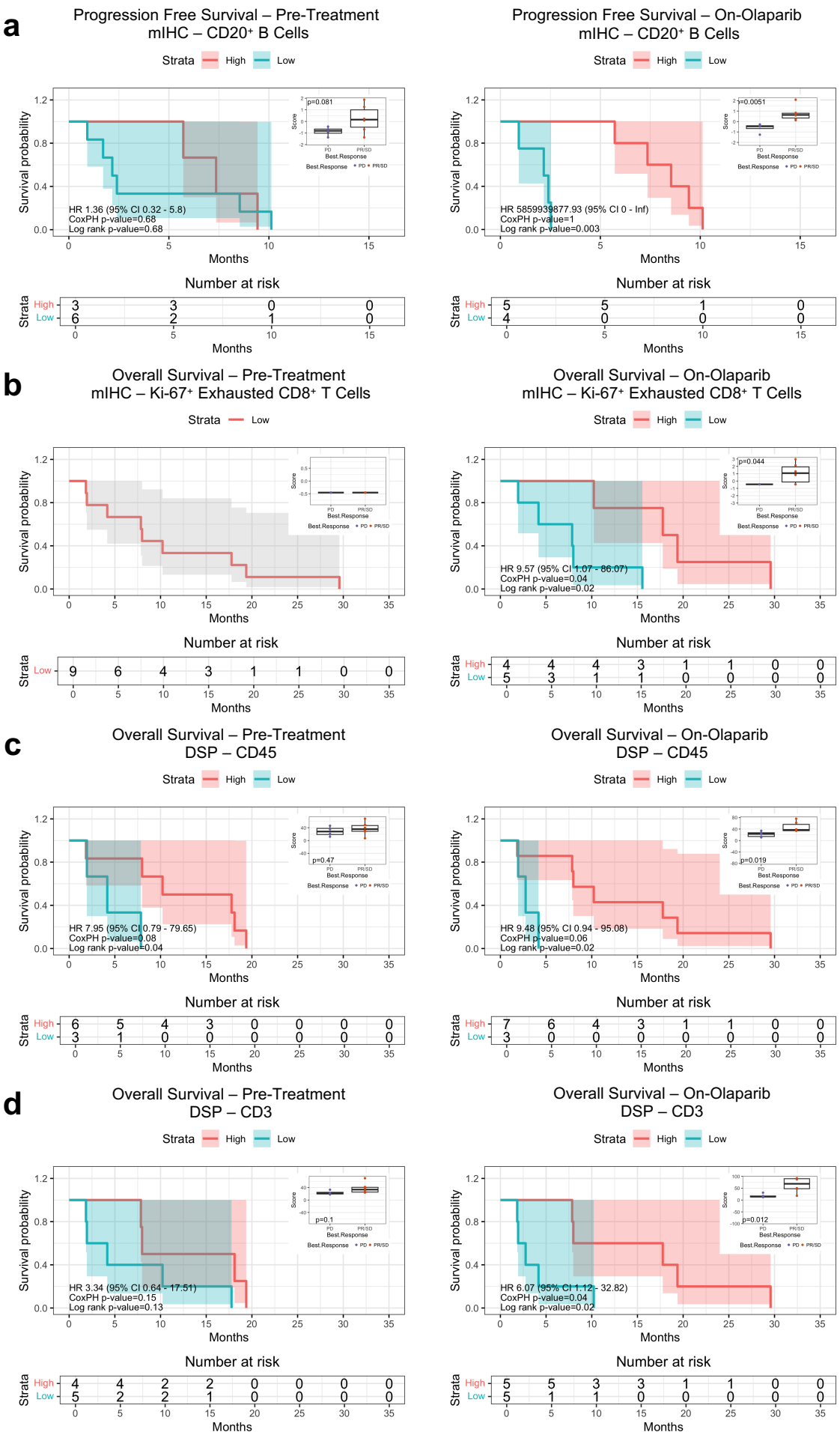

Figure 5

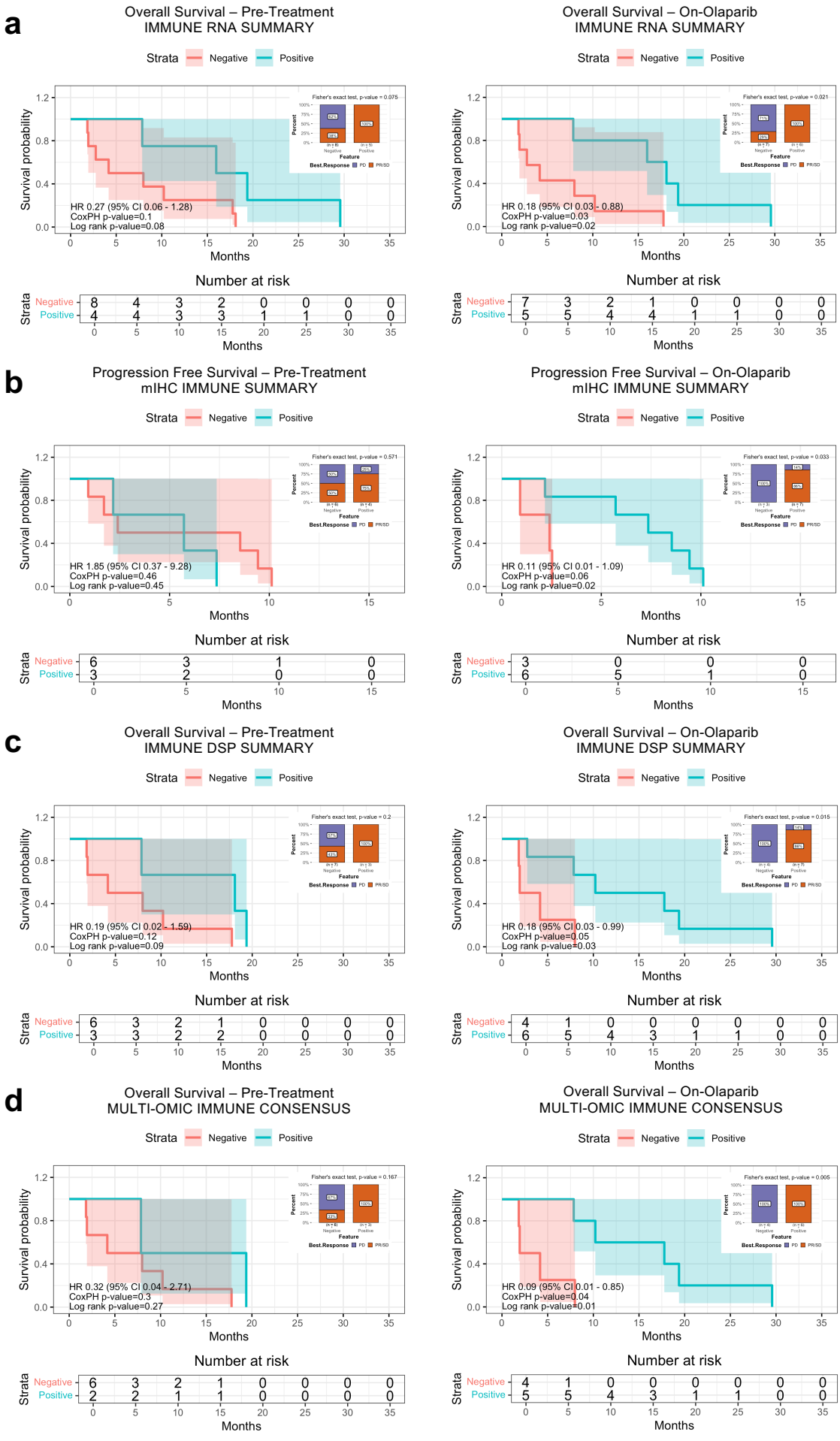

Figure 6

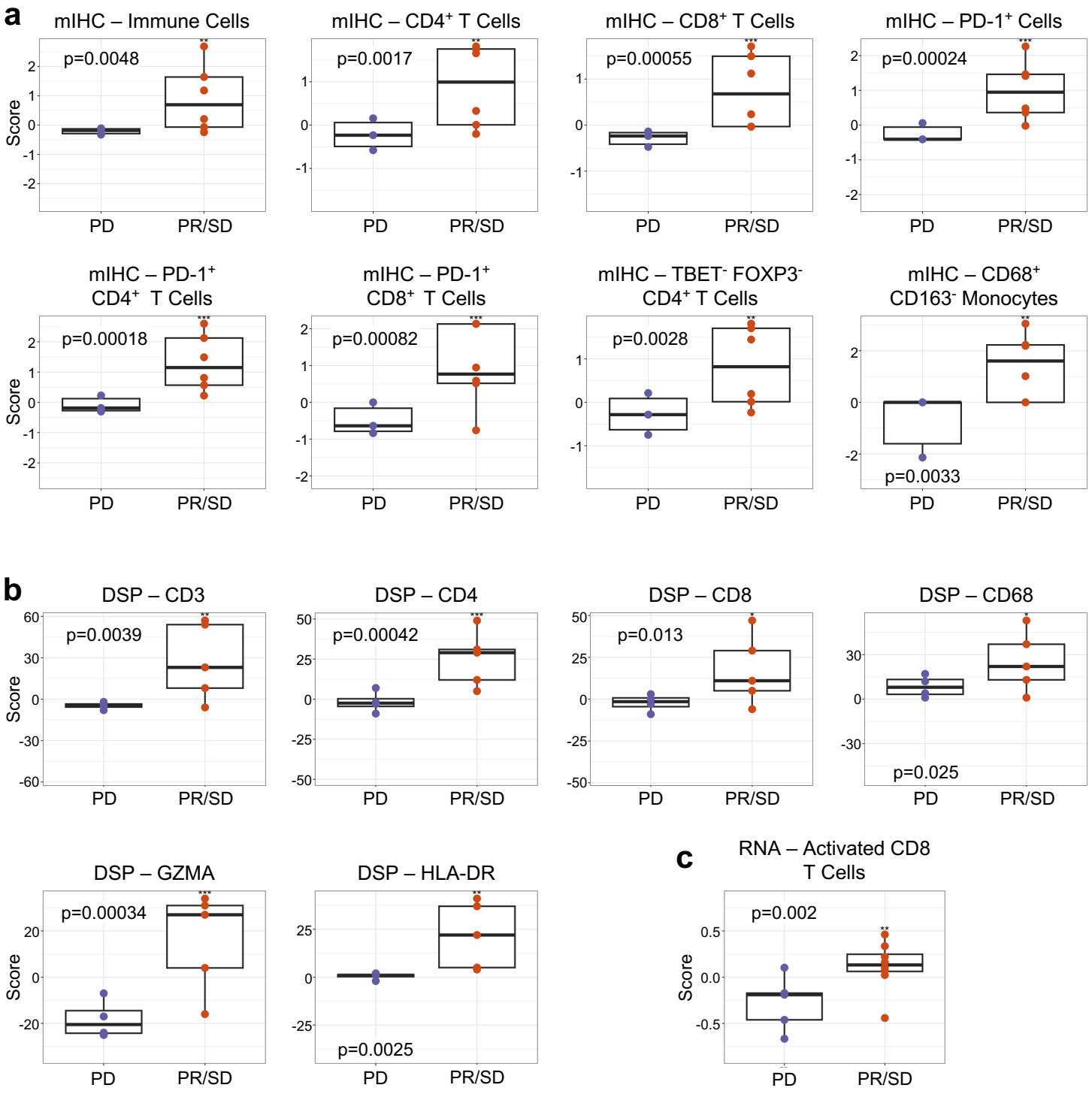

Figure 7